Direct Photon-by-photon Analysis of Time-Resolved Pulsed Excitation Data using Bayesian Nonparametrics

Meysam Tavakoli,[†] Sina Jazani,[‡] Ioannis Sgouralis,[¶] Wooseok Heo,[§] Kunihiko Ishii,[‖] Tahei Tahara,[‖] and Steve Pressé[*,⊥]

†*Department of Physics, Indiana University-Purdue University, Indianapolis, IN, USA,*

Author with equal contribution

‡*Center for Biological Physics, Department of Physics, Arizona State University, Tempe, AZ 85287,*

Author with equal contribution

¶*Center for Biological Physics, Department of Physics, Arizona State University, Tempe, AZ 85287*

§*Molecular Spectroscopy Laboratory, RIKEN, 2-1 Hirosawa, Wako, Saitama 351-0198, Japan*

‖*Molecular Spectroscopy Laboratory, RIKEN, 2-1 Hirosawa, Wako, Saitama 351-0198, Japan,*

Ultrafast Spectroscopy Research Team, RIKEN Center for Advanced Photonics (RAP), 2-1 Hirosawa, Wako, Saitama 351-0198, Japan

⊥*Center for Biological Physics, Department of Physics,*

Arizona State University, Tempe, AZ 85287, USA and

School of Molecular Sciences,

Arizona State University, Tempe, AZ 85287, USA

E-mail: spresse@asu.edu

Abstract

Lifetimes of chemical species is typically estimated, on a pixel-by-pixel basis by either fitting time correlated single photon counting (TCSPC) histograms or, more recently, through phasor analysis from time-resolved photon arrivals. While both methods yield lifetimes in a computationally efficient manner, they have limitations. First, both TCSPC and phasor analysis set the number of chemical species by hand before lifetimes can be determined. Yet the number of species itself is encoded in photon arrival times and need not be set by hand *a priori*. Next, even to determine lifetimes under the assumption of a known number of species, both methods rely on heavy data post-processing of the signal thereby requiring large amounts of data to retrieve lifetimes. As a result, the sample is exposed to orders of magnitude more light than is required and the ability to resolve fast processes is compromised. Here we propose a direct photo-by-photon analysis of data drawn from pulsed excitation experiments to infer, simultaneously and self-consistently, the number of species and their associated lifetimes from as little as a few thousand photons for two species. We do so by leveraging new mathematical tools within the Bayesian nonparametric (BNP) paradigm that we have previously exploited in the analysis of single photon arrivals from single spot confocal microscopy. We benchmark our method on simulated as well as experimental data for one, two, three, and four species with data sets from both immobilized and freely diffusing molecules.

INTRODUCTION

Fluorescence microscopy provides a means to selectively monitor the dynamics of fluorophores or labeled molecules .[1,2] Some fluorescence approaches—such as confocal microscopy,[3] two-photon microscopy[4] and super-resolution widefield applications[5]—use constant illumination to provide information on chemical kinetics,[6–8] diffusional dynamics[9–11] or spatial locations of molecules.[12,13] Other methods use pulsed illumination[14–18] or illumination intensity modulated at a fixed frequency[18–23] where photon arrival times encode critical information, say, on the excited state lifetime or the number of different chemical species. This is the basis of lifetime imaging[13,24–27] that has been used to reveal information on local pH,[28,29] oxygenation[28] and other cellular metabolic traits[23,30] affected by cellular microenvironments.

In pulsed illumination,[31,32] photon arrival times are analyzed,[33–36] under the assumption of a known number of molecular species with unknown lifetimes to be determined.[37,38] Methods of analysis include Bayesian approaches given known species numbers.[39–43] A common analysis starting point is the photon arrival histogram termed the time-correlated single photon counting (TCSPC) histogram.[2,44–46] These histograms are typically fitted using multi-exponentials[37,47] to identify the lifetime of each species. That is, lifetimes, τ_m, and the weights of the mth lifetime component, a_m, are modeled and determined using multi-exponential decay fits (Eq. 1)

$$I(t) = \sum_{m=1}^{M} a_m \exp\left(-\frac{t}{\tau_m}\right) \tag{1}$$

where $I(t)$ is the intensity of photons at time t. The number of exponential components, M, can be pre-specified according to some goodness-of-fit metric to avoid over-fitting[41] that we discuss in the Supplementary Information. While such methods yield lifetimes in a computationally efficient manner, they have key limitations. First is the requirement that the number of species, M, be pre-specified as it otherwise *cannot* be learned independently although, in principle, it is encoded in the data. Yet learning the number of species itself may

be useful as the number of chemical species may be unknown prior to collecting data for a number of reasons.[48–51] Additionally, as we will show, these methods can be data *inefficient*. The latter drawback is especially problematic if: temporal resolution is important; the sample is light sensitive; multiple lifetimes are fairly similar requiring long photon arrival traces to discriminate one from the other.

When illuminating a sample by modulating light intensity at a fixed frequency,[21,52–55] the emission is also modulated but otherwise phase shifted.[18,56] For a modulation frequency of ω, the measurements may be used to obtain a phase shift, ϕ, and an intensity modulation ratio, m (see Fig. S9). The phase shift and intensity modulation ratio, in turn, determine two coordinates (G, S) of a "phasor plot" in the following way

$$G(\omega) = m\cos\phi \quad \text{and} \quad S(\omega) = m\sin\phi. \tag{2}$$

Lifetime values of the emissive fluorophores can then be deduced from the point on which they appear on the phasor plot.[57–59] Phasor analysis is especially intuitive as it allows one to immediately deduce whether more than one lifetime component is present.[60,61] In particular, mono-exponential lifetimes fall somewhere on the semicircle of radius 1/2 beginning at coordinate (1,0) and moving counterclockwise to (0,0). Deviations thereof imply a mixture of lifetimes. Full details are provided in the Supplementary Information. A variant of phasor analysis also holds for pulsed excitation.[49,57,62] The advantages and drawbacks of phasors analysis are similar to those of TCSPC in that the number of species must be known in advance. What is more, the retrieval of lifetime information from phasor analysis requires independent knowledge of not only the number of species but also the lifetime of all but one unknown species whose lifetime is to be determined from a mixture of chemical species.[27,57,63,64]

To summarize, TCSPC and phasor analysis learn lifetimes at minimal computational

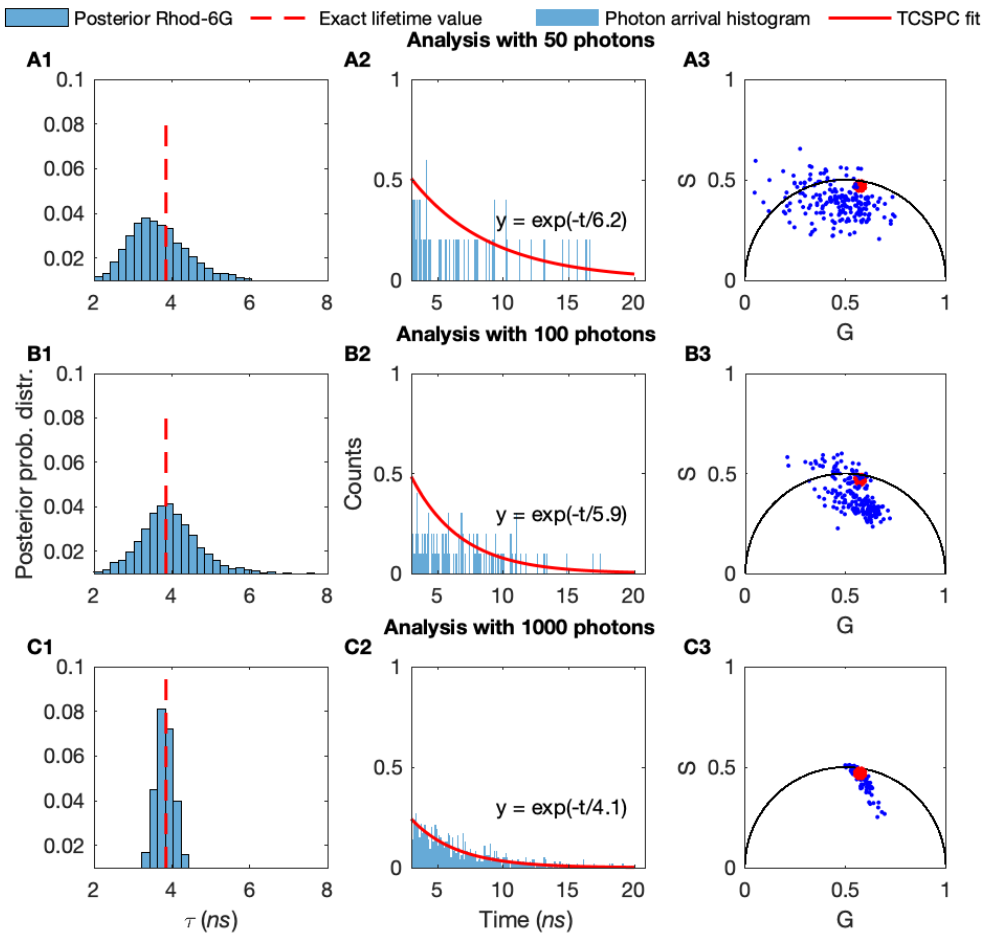

Figure 1: **TCSPC and phasor analysis reveal excited state lifetimes provided a large number of photons are available.** Preliminarily, here we compare our method relying on Bayesian nonparametrics (BNPs) which we compare in greater depth later to TCSPC and phasor analysis with limited data available for analysis. (A1-A3) Here we use just 50 photons from experimental time trace Rhod-6G to compare all three methods: (A1) BNPs, $\tau_{BNP} = 3.10\ ns$, (A2) TCSPC, $\tau_{TCSPC} = 6.20\ ns$ with $\chi^2 = 11.27$, and (A3) phasor analysis, $\tau_{phasor} = 5.96\ ns$. Given 100 photons in (B1-B3) we obtain $\tau_{BNP} = 3.95\ ns$, $\tau_{TCSPC} = 5.90\ ns$ with $\chi^2 = 5.24$, $\tau_{phasor} = 5.10\ ns$. Finally, given 1000 photons in (C1-C3) we obtain $\tau_{BNP} = 3.91\ ns$, $\tau_{TCSPC} = 4.10\ ns$ with $\chi^2 = 1.12$, $\tau_{phasor} = 3.94\ ns$.

cost provided the number of species is known. At higher computational cost, we could learn not only the number of species, but even full joint distributions over the possible number of species as well as their associated lifetimes which we know to be encoded in the photon arrivals. In order to do so, however, we need to relinquish the traditional (parametric) Bayesian paradigm that assumes a fixed model structure (i.e., a fixed number of species). Ideally, we would like to achieve this with the same number or fewer photons than is required in TCSPC and phasor analysis to reveal the lifetimes alone; see Fig. 1.

We have previously exploited the Bayesian nonparametric (BNP) paradigm[65–68] to analyze single photon arrival traces in order to learn diffusion coefficients from minimal photon numbers drawn from single spot confocal experiments.[10,69] Traditionally, such photon arrivals were analyzed using tools from fluorescence correlation spectroscopy where very long traces were collected and auto-correlated in time. Just as with this the problem at hand, the direct photon-by-photon analysis demanded a different approach as the stochastic number of molecules contributing photons was unknown and an estimate of that number deeply impacted our diffusion coefficient estimate. It is for this reason that we invoked the nonparametric paradigm there.

Similarly, the BNP paradigm is also required to infer the number of species and their associated lifetimes. This is because assuming an incorrect number of species leads to incorrect lifetime estimates for each species; see Fig. 2.

In the "normal" (i.e., parametric) paradigm, we assume models and, given these models, write down likelihoods used in data analysis. These parametric approaches[70–73] are irrelevant to the current analysis where both the number of species and their associated lifetimes are unknown. Put differently, BNPs reshape our interpretation of biophysical data. Just as we treat model parameters as random variables in the parametric Bayesian paradigm, within the BNP paradigm, we treat models themselves as the random variables and try to learn full posterior distributions over the number of species.

Here we propose a method that exploits BNPs[74,75] to learn species and their associated

lifetimes with as few photons as possible using pulsed illumination. As with any inverse methods, in BNPs we start from the data: namely the time lag between the peak of the pulse and the detection time of the photon termed "microtime" discussed in more detail later in . To be precise, each species is defined as contributing photons some time after pulsing dictated by an exponential distribution with a decay constant (lifetime) unique to that species.

The advantages of our method are four-fold: 1) we can learn the number of species; 2) by resolving lifetimes and species with fewer photons, we can minimize photo-damage; 3) as a corollary to the previous point, we can monitor processes out-of-equilibrium where only few photons are available before chemical conversion into another species; 4) given long traces, we can exploit the additional data, if need be, to discriminate between species of similar lifetimes that could not otherwise be previously discerned.

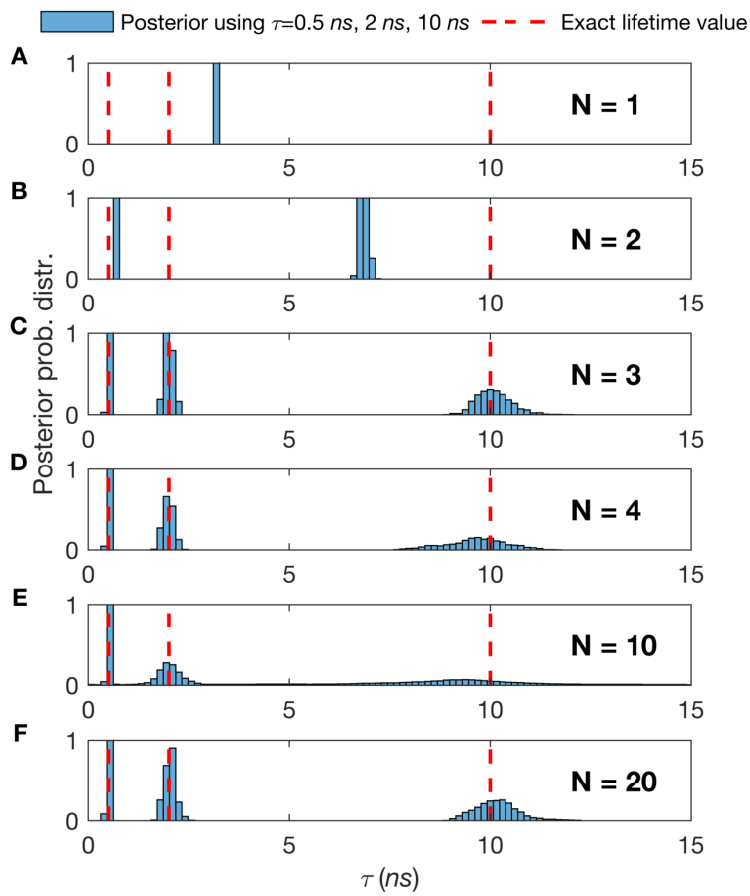

Figure 2: **The number of species assumed in the analysis directly impacts the lifetimes ascribed to those species. Thus, we need an independent method to estimate species numbers.** (A-F) We generate synthetic traces with three species with a total of 2×10^4 photon arrivals and lifetimes, τ, of 0.5 ns, 2 ns, and 10 ns. To estimate the τ within the normal (i.e., parametric) Bayesian paradigm, we start by assuming the following number of species, $N = 1$ (A), $N = 2$ (B), $N = 3$ (C), $N = 4$ (D), ..., $N = 10$ (E), ..., and $N = 20$ (F). The good fit provided by $N > 2$ and the mismatch in the peak of the posterior distribution over the lifetime and correct value of the lifetime (red dotted line) in all others underscores why it will become critical for us, or any method analyzing single photon data in the context of confocal microscope experiments, to correctly estimate the number of species contributing to the trace in order to deduce chemical parameters such as lifetime.

RESULTS

Our goal is to characterize quantities that describe molecular chemistry at the data-acquisition timescales of TCSPC with a focus on obtaining lifetime estimates and the number of chemical species. In order to estimate lifetimes, we also estimate intermediate quantities, such as the fraction of different species contributing photons as detailed in the method section.

Within the BNP approach,[76–78] our estimates take the form of posterior probability distributions over unknown quantities. These distributions combine parameter values, probabilistic relations among different parameters, as well as the associated uncertainties. To quantify this uncertainty, we calculate a posterior variance and use this variance to construct error-bars (i.e., credible intervals). As follows from Bayesian logic, the sharper the posterior, the more conclusive (and certain) the estimate.[69,76,79]

We first validate our approach on synthetic data where the ground truth is available. We then test our method on experimental data. For the latter case, we compare our analyses to the results obtained from both TCSPC and phasor plot methods.

Method Validation using Synthetic Data

To show the robustness of our method, we generate synthetic traces for immobilized molecules with: i) variable data set sizes, Fig. 3 involving multiple species, Fig. 4; ii) variable fraction of molecules contributing photons from different species, Fig. 5; and iii) variable difference of lifetimes for mixtures of lifetimes, Fig. 6. All parameters not explicitly varied are held constant across all figures. The parameters not varied are held fixed at the following baseline values: lifetime between 1 ns and 10 ns which is the typical lifetime range of a fluorophore,[18,80] two species which is most frequent in related studies,[18,19,23] and fraction of molecules contributing photons from different species set at 50% : 50%.

Also, in the Supplementary Information, we worked with cases involving three and four different species (as opposed to a just one or even two species) as this scenario presents the

greatest analysis challenge because very few photons, and thus little information, is gathered on each species. In a similar spirit, we also default to short traces that cannot meaningfully be analyzed using TCSPC and phasor approaches as illustrated in Fig. 1. As the mathematics remain unaffected, and this scenario reflects the reality of many experiments, we show in the Supplementary Information, Figs. S1 and S2, results for freely diffusive molecules.

Number of photons

We benchmark the robustness of our approach with respect to the length of the trace (i.e., the total number of photon arrivals) at fixed number of species, lifetime, and molecule photon emission rate. The first important conclusion is that, for the values of parameters selected, we need at least one order of magnitude less data than both TCSPC and phasor analysis; see Fig. 1. For instance, to obtain an estimate of the lifetime within 10% of the correct result in the one species case, our method requires ≈ 100 photons (emitted from the species of interest), while both TCSPC and phasor require ≈ 1000 photons to determine the lifetime to within the same error bar. In the case of two species traditional approaches need at least 3×10^4 photons in comparison to ≈ 3000 for our proposed BNP approachs; see Figs. 3 and 4.

To determine how many photons were required for our method, we chose the mean value of the lifetime posterior, and measure the percentage difference of this mean to the ground truth known for these synthetic traces. For both TCSPC and phasor analysis of one species lifetime, ≈ 1000 photons were required to achieve the same accuracy as our approach which required ≈ 100 photons. For the case of a mixture of two species, this number rose to 10^4 or more photons for both TCSPC and phasor analysis but rose only to ≈ 3000 photons for our method;[70,81] see Fig. 7.

In general, the difference in the photon numbers demanded by our method and traditional analysis depends on a broad range of experimental parameter settings. This is the reason why, throughout this work, we explore different settings—holding all other settings fixed—in subsequent subsections as well as the Supplementary Information.

Another important concept, illustrated in Figs. 1, 3, and 4 that will keep re-appearing in subsequent sections, is the concept of a photon as a *unit of information*. The more photons we have, the sharper our lifetime estimates. This is true, as we see in these figures, for increasing trace length. Similarly, as we will see in subsequent subsections, we also collect more photons as we increase the contribution of labeled molecules (and thus the number of molecules contributing photons to the trace).

Mixtures of different species contributing photons

To test the robustness of our method when different species contribute an uneven number of photons, we simulate data with 70% of the population in species 1 and 30% in species 2 (Fig. 5A). We also considered fractions of contributing molecules from different species of 50% : 50% (Fig. 5 B), and 30% : 70% (Fig. 5 C). For all cases, the lifetimes were fixed at 1 ns and 10 ns for ≈ 3000 photon arrivals. Fig. 5 summarizes our results and suggests that posteriors over lifetimes are broader—and thus the accuracy with which we can pinpoint the lifetimes drops—when the contribution of labeled molecules is lower. Intuitively, we expect this result as fewer species within the confocal volume provide fewer photons and each photon carries with it information that helps refine our estimated lifetimes.

Lifetime resolution

We repeat the simulations with two species and ask about how many photons are required to resolve similar lifetimes. Here, we have presented the dependency of the time resolution to the number of collected photons in Fig. 6. As expected, the number of photons required to resolve increasingly similar lifetimes grows as the ratio of lifetimes approaches unity. However, this also suggests that if we were to resolve species of similar lifetimes, we could use the amount of data typically used in TCSPC or phasor analysis to resolve these while TCSPC or phasor analysis would still require an additional order of magnitude more data. As we noted earlier, both TCSPS and phasor analysis must impose by hand the number of

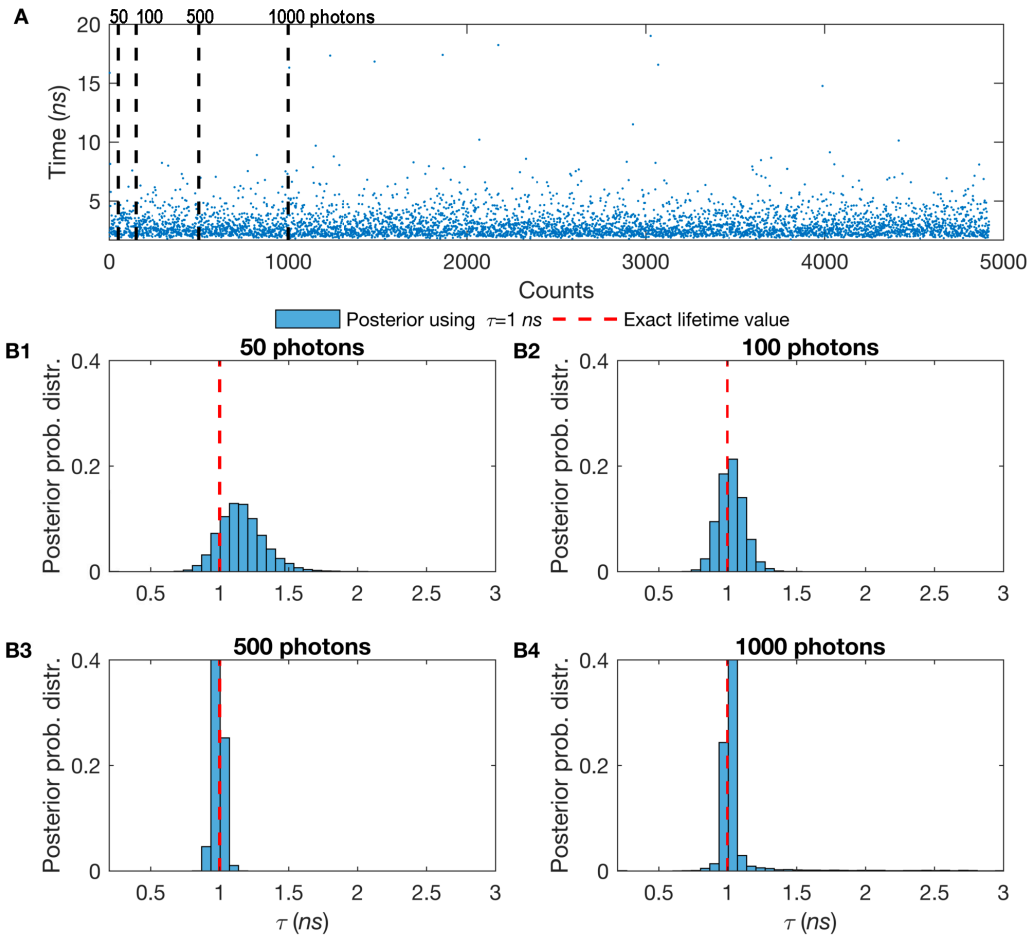

Figure 3: **The greater the number of detected photons, the sharper the molecular lifetime estimate.** (A) Here, we work on single species lifetime while all molecules are immobilized. The synthetic trace generated using a lifetime of $\tau = 1\ ns$. The blue dots represent single photon arrival times (y-axis) recorded after each excitation pulse (x-axis). We consider the excitation pulse as a Gaussian IRF (Eq. 4) occurs at a frequency of 40 MHz with standard deviation of 0.1 ns. (B1) In the analysis to determine lifetimes, we first start with just 50 photons, first black-dashed line in panel (A), and gradually increase the number of photons considered in the analysis to (B2) 100, second black-dashed line in panel (A), (B3) 500, third black-dashed line in panel (A), and (B4) 1000 photons, last black-dashed line in panel (A). The ground truth for the lifetime is known (as this is synthetic data) and it is shown by the red-dashed line.

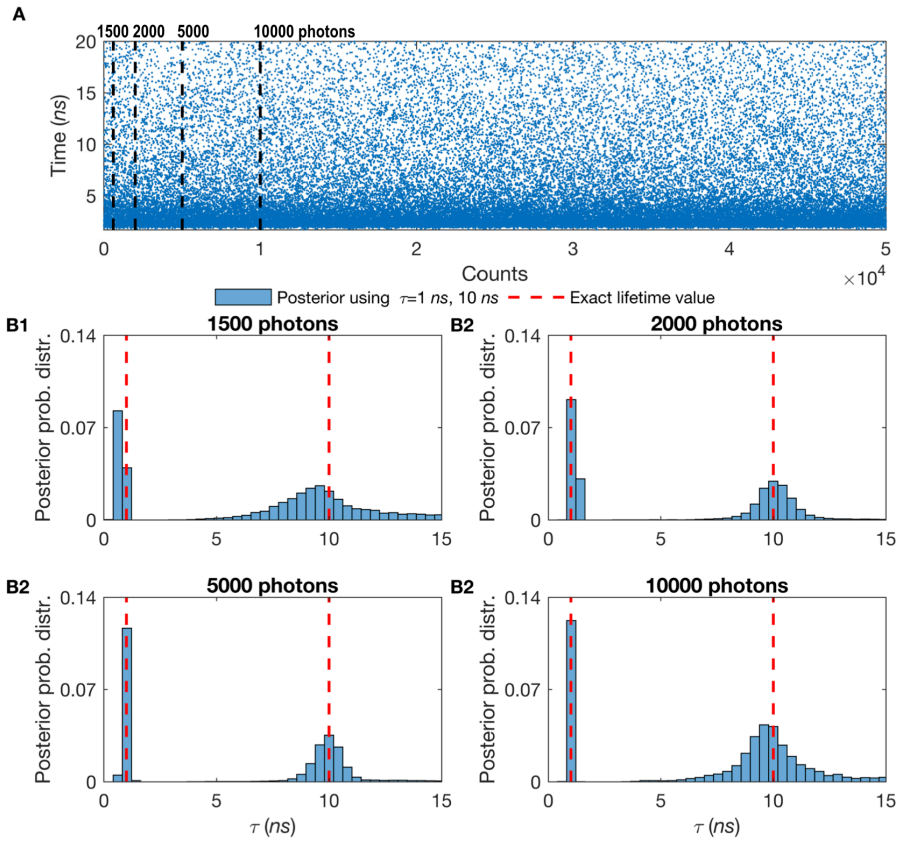

Figure 4: **Effect of the number of detected photons on two simultaneous molecular lifetime estimates. The more photons collected, the sharper the lifetime estimate for the case of two species.** (A) Here, we use mixtures of two species with different lifetimes while all molecules are immobilized. The synthetic data is generated using $\tau = 1\ ns$ for the first species and $\tau = 10\ ns$ for the second with equal ratio of molecules of each species ($50\% - 50\%$). The blue dots represent single photon arrival times detected after each excitation pulse. (B1) In the analysis to determine both lifetimes, we first start with just 1500 photons, first dashed line in panel (A), and gradually increase the number of photons to 2000 (B2), 5000 (B3), and 10000 (B4) photons. Here, all other features such as the frequency of acquisition and width of pulse are the same as in Fig. 3. Also, we follow the same red-dashed line convention as in 3. To see the results for more than two species see the Supplementary Information, Figs. S4 and S5.

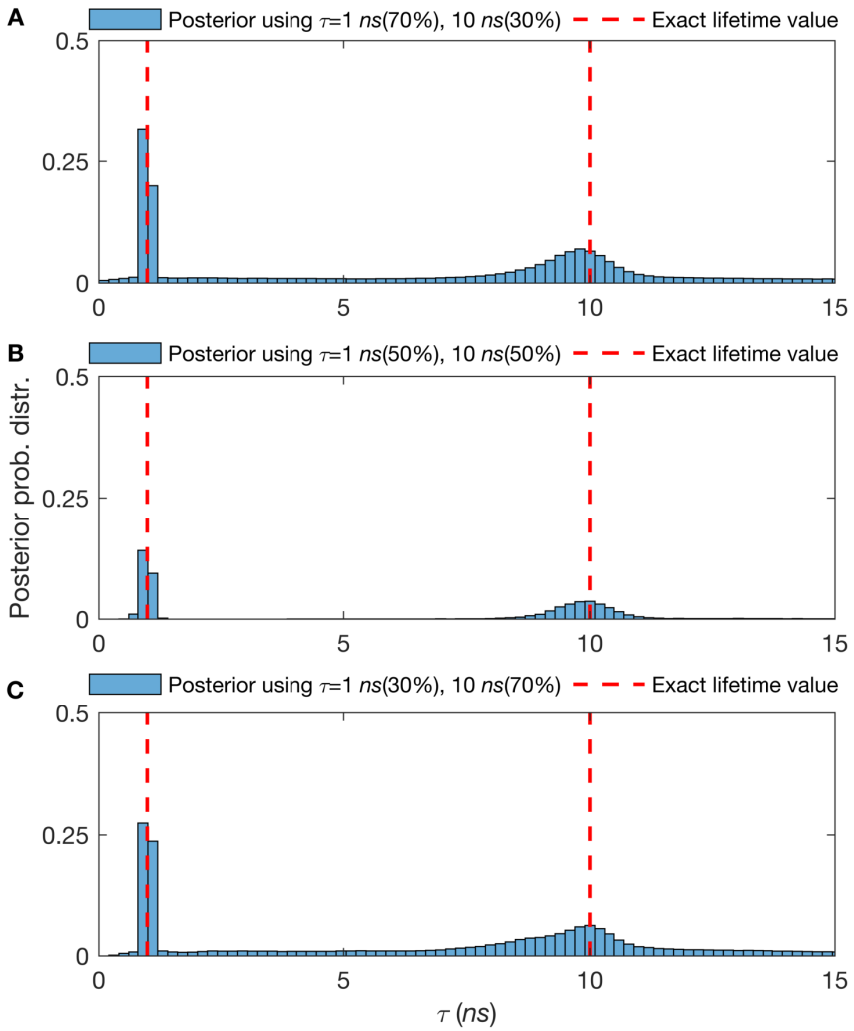

Figure 5: **Effect of the relative fraction of contributing molecules from different species on molecular lifetime estimates. Higher molecular contributions provide more photons per unit time and thus sharper lifetimes estimates**. (A-C) The posterior probability distributions of traces with lifetimes of 1 ns and 10 ns, with 3000 total photons and fraction of contributing molecules from different species of $70\% - 30\%$, $50\% - 50\%$ and $30\% - 70\%$ respectively. Here, all other features such as the frequency of acquisition and width of pulse are the same as in Fig. 3. Also, we follow the same red-dashed line convention as in 3. For more details see Supplementary Information Fig. S6.

species while, in our method, the number of species are learnt. Moreover, if we know number of species we require even fewer photons that we mentioned earlier.

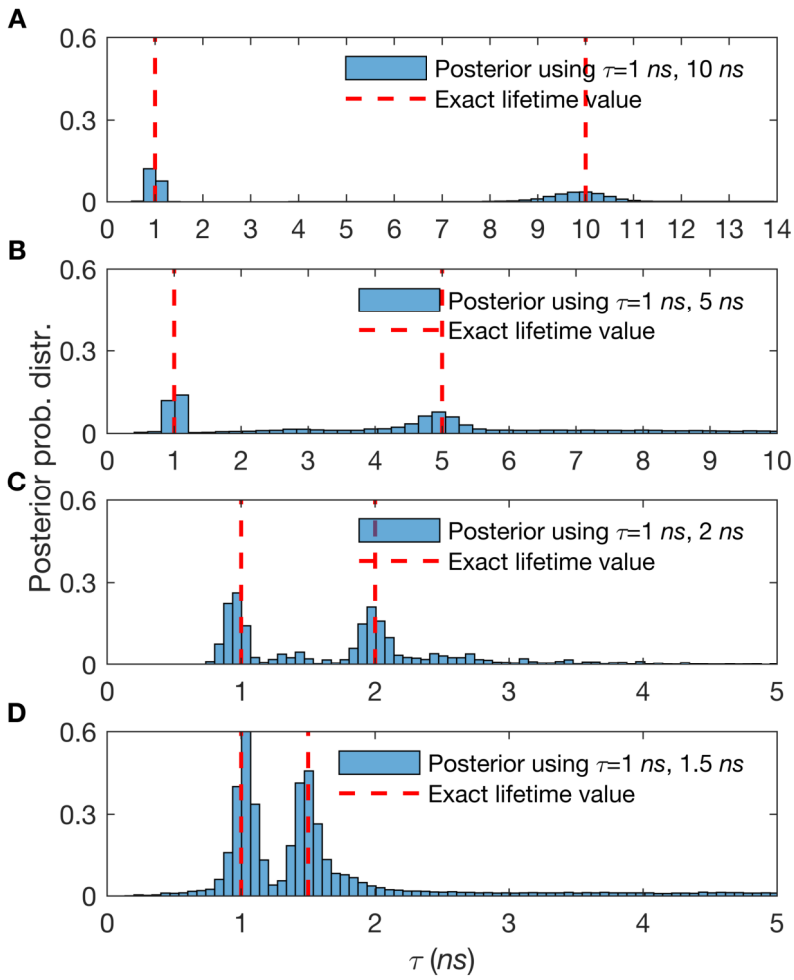

Figure 6: **Lifetime resolution for double species lifetimes.** Here we show posterior probability distributions over estimated lifetimes. In The synthetic traces acquired contain 3000 to 20000 photon arrivals and start in (A) with well separated lifetimes of 1 ns and 10 ns ($\approx$ 3000 photons) before gradually considering less well separated lifetimes such as in (B) where the lifetimes are 1 ns and 5 ns ($\approx$ 3000 photons), in (C) where the lifetimes are 1 ns and 2 ns ($\approx$ 10000 photons), and in (D) where the lifetimes are 1 ns and at last 1.5 ns ($\approx$ 20000 photons). The fraction of molecules contributing photons from different species is even split ($50\% - 50\%$). Here, all other features, such as the frequency of acquisition and width of pulse, are the same as in Fig. 3. Also, we follow the same red-dashed line convention as in 3.

Estimation of physical parameters from experimental data

To evaluate our approach on real data, we used experimental data collected under a broad range of conditions. That is, we used measurements from different fluorophores, namely Cy3, TMR, Rhod-B, and Rhod-6G. The lifetimes for these dyes are determined from TCSPC using the entire trace and are compared with values published in the literature.[82–85] Figs. 7 and 8 were collected using the Rhod-B and Rhod-6G dyes and these results were used to benchmark the robustness of our method on individual species as well as mixtures of species with a variable fraction of chemical species contributing photons. In the Supplementary Information, Fig. S7, we show more experimental results for cases involving more than two species.

In Fig. 1, we verified our method on Rhod-6G with respect to the total number of photon arrivals. The first important conclusion is that we need at least one order of magnitude less data than both TCSPC and phasor analysis to obtain an estimate of the lifetime within 10% of the correct result. That is, we need ≈ 100 photons, while both TCSPC and phasor require ≈ 1000 photons. For two or more species, the situation for both TCSPC and phasor grows more challenging for two reasons. First, the number of species cannot be independently determined and, even if known, at least ≈ 10000 photons are required to determine lifetimes to within 10% of the correct result (as detailed in Section "Number of photons"). Moreover, for all cases, we determined the ground truth (red-dashed lines) from TCSPC using the whole trace with all photons available. To be clear, we learn the number of species directly using BNPs and do not assume a number ahead of time.

In general, the difference in the photon numbers demanded by our method and traditional analyses depend on a broad range of experimental parameter settings. This is the reason, we explore different settings—holding all other settings fixed—just as we did with synthetic data in subsequent subsections as well as the Supplementary Information.

Benchmarking on experimental data using a different number of photons for mixtures of Rhod-B and Rhod-6G

Similarly to the synthetic data analysis appearing in Fig. 4, we benchmark the robustness of our approach with respect to the length of the trace (i.e., the total number of photon arrivals) given fixed lifetimes and fraction of chemical species contributing photons at 50% : 50%. Again the important conclusion is that, for the values of parameters selected, we need at least one order of magnitude less data than both TCSPC and phasor analysis; see Fig. 1 for the analysis of one species, Rhod-6G, and Fig. 7 for the analysis of two species. For instance, to obtain an estimate of the lifetime to within 10% of the correct result for the case of two species, our method requires ≈ 3000 photons, while both TCSPC and phasor require $\approx 3 \times 10^4$ photons.

Benchmarking on experimental data using different fractions of Rhod-B and Rhod-6G

We start by evaluating our method on mixtures of Rhod-B and Rhod-6G but present in different amounts. Similarly to Fig. 5 for the analysis of two species from synthetic data, we show estimates of the lifetimes for two species, Rhod-B and Rhod-6G, present at 70% : 30% fraction (Fig. 8A), at 50% : 50% fraction (Fig. 8B), and at 30% : 70% fraction (Fig. 8C). Fig. 8 summarizes our results and suggests that posteriors over lifetimes are broader—and thus the accuracy with which we can pinpoint the lifetimes drops—when the contribution from the dye concentration for that species is lower. Just as before, we need at least one order of magnitude less data than both TCSPC and phasor analysis; see Fig. 8. For instance, to obtain an estimate of the lifetime to within 10% of the correct result, our method requires $\approx$ 3000 photons directly emitted from the dye, while both TCSPC and phasor analyses become more challenging and for two species case requires at least $\approx 3 \times 10^4$ photons (assuming the number of species is known). In the Supplementary Information, we show additional results for the case of three and four species with different fractions of chemical species contributing

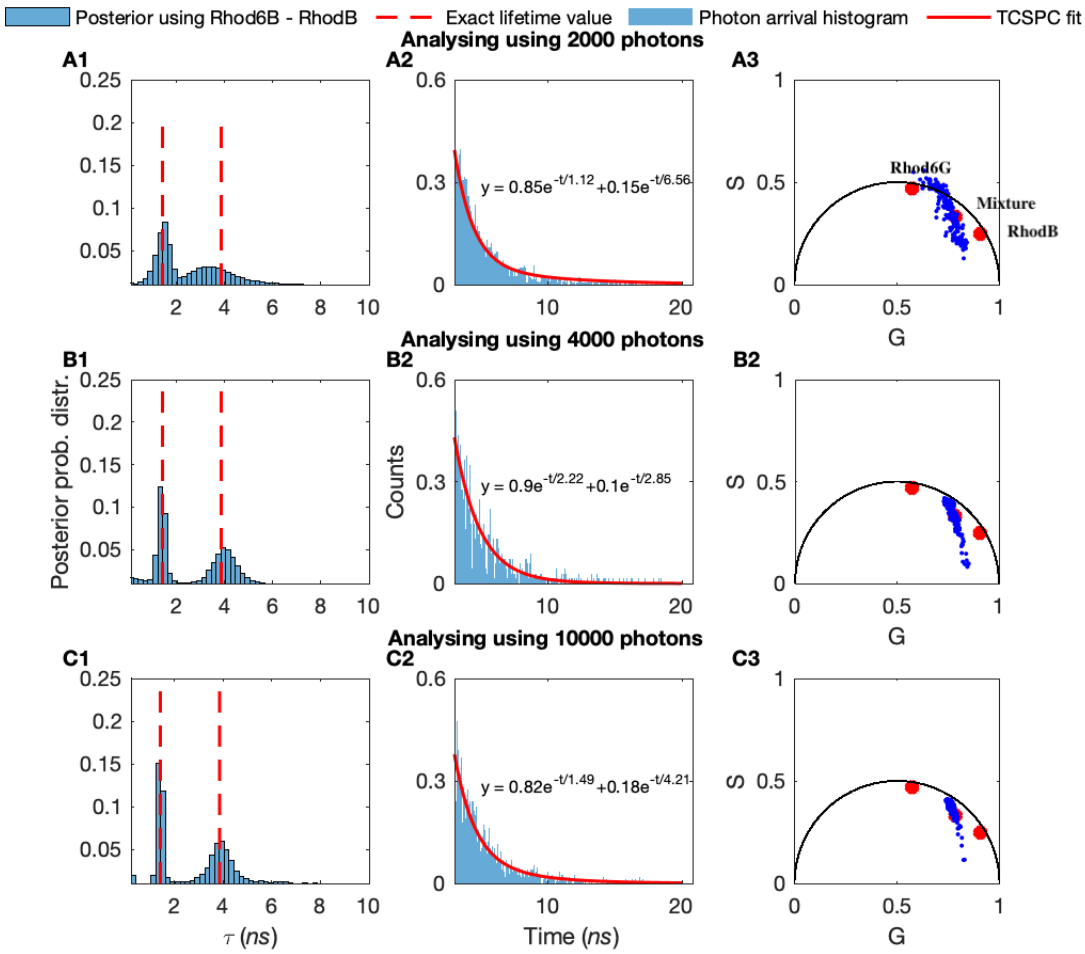

Figure 7: **Comparison of the number of photons needed to assess the lifetimes of mixtures of Rhod-B and Rhod-6G.** In (A1-A3) we use 2000 photons and compare all three methods: (A1) BNPs, (A2) TCSPC, and (A3) phasor analysis. In (B1-B3) and (C1-C3) we repeat the analysis for 4000 and then 10^4 photons. The estimated lifetimes are (A1) BNPs, $\tau_{BNP} = 1.44, 3.39\ ns$, (A2) TCSPC, $\tau_{TCSPC} = 1.12, 6.56\ ns$ with $\chi^2 = 1.17$. In (B1-B2), $\tau_{BNP} = 1.42, 3.96\ ns$, $\tau_{TCSPC} = 2.22, 2.85\ ns$ with $\chi^2 = 3.21$, and (C1-C2), $\tau_{BNP} = 1.41, 3.90\ ns$, $\tau_{TCSPC} = 1.49, 4.21\ ns$ with $\chi^2 = 1.19$. The ground truth (red-dashed lines) is obtained using TCSPC when analyzing the whole time trace. In our BNP analysis, we do not pre-specify the number of species, we learn them.

photons where the number of photons required for the analysis grows substantially in phasor and TCSPC analysis.

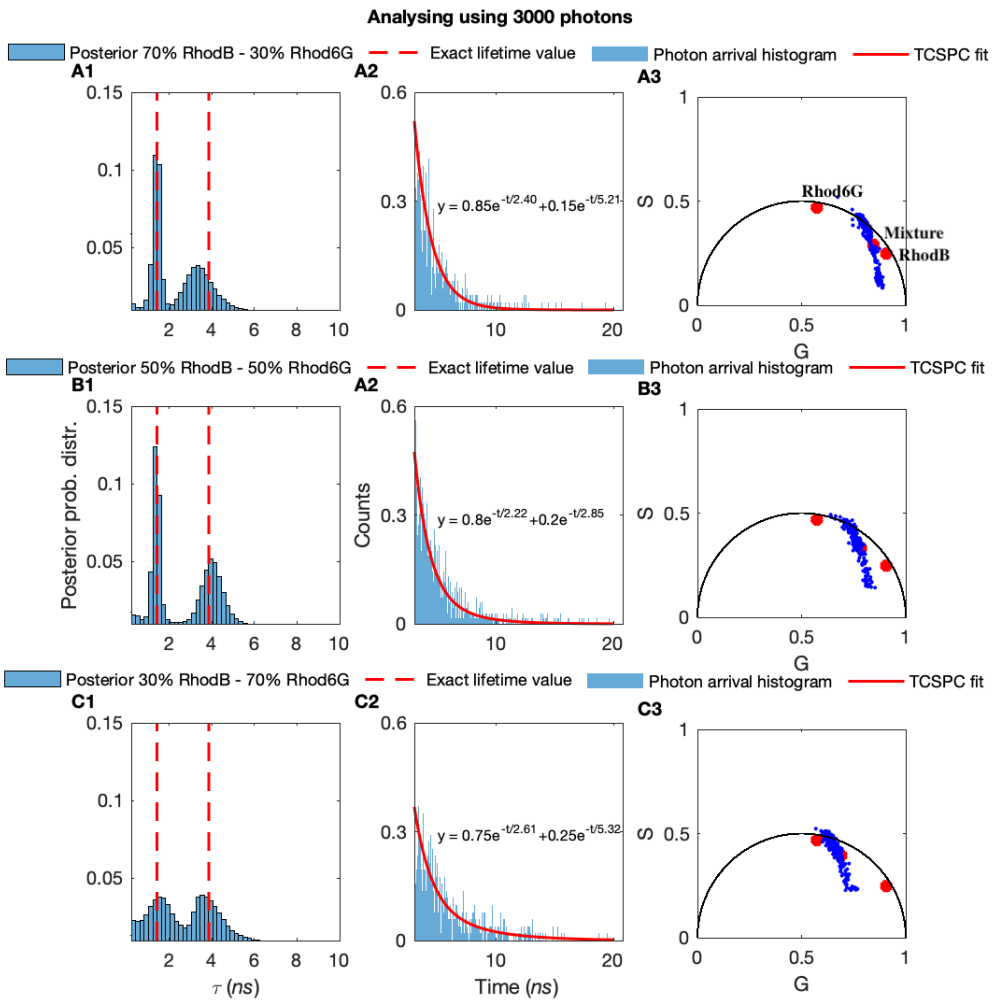

Figure 8: **Effect of the fraction of molecules contributing photons from different species on molecular lifetime estimates. Higher molecular contributions provide more photons per unit time and thus sharper lifetime estimates**. (A1-A3) The experimental trace is selected using two species, Rhod-B and Rhod-6G, with a total of about 3000 photon arrivals with fraction of molecules contributing photons from different species $(70\% - 30\%)$. (A1) BNPs, (A2) TCSPC, and (A3) phasor estimations. In (B1-B3) and (C1-C3) we repeat the analysis for fraction of $(50\% - 50\%)$ and $(30\% - 70\%)$ The estimated lifetimes are (A1) BNPs, $\tau_{BNP} = 1.44, 3.39\ ns$, (A2) TCSPC, $\tau_{TCSPC} = 1.40, 5.21\ ns$ with $\chi^2 = 3.73$. In (B1-B2), $\tau_{BNP} = 1.42, 3.96\ ns$, $\tau_{TCSPC} = 2.22, 2.85\ ns$ with $\chi^2 = 2.89$, and (C1-C2), $\tau_{BNP} = 1.41, 3.90\ ns$, $\tau_{TCSPC} = 2.61, 5.32\ ns$ with $\chi^2 = 4.15$.

DISCUSSION

Across all spectroscopic and imaging applications, the photon is the basic unit of information.[69,86] Decoding information directly from single photon arrivals, with as few photons as possible without binning or correlating or other pre-processing of the data, is the main focus of our data-centric analysis strategy. Yet decoding information directly from single photon arrivals presents fundamental model selection problems.

For example, in the case of FCS, if we are to learn diffusion coefficients directly from limited photon arrivals, we must know how to write down a likelihood or, put differently, we must know the number of molecules contributing photons that, in turn, dictate the form for the likelihood.[69] As we do not know how many molecules we have, and what the appropriate likelihood should be, we have a model selection problem. Similarly, for lifetime imaging, if we are to learn the lifetime of the chemical species contributing photons, we must also know the number of species in order to write down a conventional likelihood.

Traditional Bayesian methods do not have a direct solution to the model selection problem[75,77] as they also require us to be able to write down a likelihood. That is, they consider a fixed model (and a fixed likelihood) and treat the model's parameters as random variables of the posterior distribution. By contrast, BNP, which are a direct logical extension of parametric Bayesian methods, treat models alongside their parameters as random variables.[65,78,87–92]

This ability to treat models themselves as random variables is the key technical innovation that prompted the development of BNPs in the first place. BNPs make it possible to avoid the computationally infeasible task of first enumerating and second comparing all models for any associated parameter values to all other competing models and their associated parameter values.

The BNP approach to tackling lifetime image analysis that we propose here cannot replace phasor analysis[20,23,53,57,59,62,93] or TCSPC[2,14,29,32,46,81] for simple one component systems on account of their computational efficiency. However, at an acceptable computational cost, BNP approaches provide a powerful alternative. They give us the ability to: determine the

number of species; use much less data to obtain lifetime estimates (and thus reduce photo-toxic damage to a light-sensitive sample); use longer photon arrival traces, if available, to tease out small differences in lifetimes between species as BNP-based methods are more data efficient; probe processes resolved on faster timescales (again, as we require fewer photons); exploit all information encoded in the photon arrivals (and thus not require separate control experiments, as needed in phasor approaches, for the measurement of the lifetime of one species to determine the lifetime of a second species when a mixture of two species, say, is present).

As for the computational cost, obtaining lifetimes (to within 10% of the ground truth lifetime for a one-species for the parameters we used in Figs. 3 and 1 requiring ≈100 photons) takes 5 minutes on a typical scientific desktop as of the publication date of this paper (based on a system with 6G RAM, Core (TM) i7-2.67 GHz CPU). For a two-species mixture, Figs. 4 and 7 , under the same parameters and requiring 3000 photons, it was a modest increase to 15 minutes. The point, here, is that the analysis of single or multi-species data *can* be performed with an average desktop computer and it does not necessarily require high performance computing facilities.

The real strength of BNP becomes clear when we reach two, three, four or possibly even more species. Beyond being able to work with low photon counts, another key advantage of our method is its flexibility. The ability to use BNP, and treat models as random variables, in lifetime imaging is the real point here and, as such, our framework can be adapted to treat a range of experimental setups.

In particular, our framework can straightforwardly be adapted to treat: any instrumental response function (IRF) by modifying Eq. 4 as appropriate; and any background photon arrival statistics or detector dark counts by modifying Eq. 5 especially relevant to *in vivo* imaging. In the Supplementary Information, Fig. S3, we tested the robustness of our method by varying the number of background photons in our data set. More significant extensions of our work, albeit generalizations that would leverage the framework at hand, would be to

consider lifetime changes, due to chemical modifications of our species, over the timescale of data acquisition as may be expected in complex *in vivo* environments.[94,95] Another is to extend our work to analyze fluorescence lifetimes over multiple spatial locations, the purview of fluorescence lifetime imaging (FLIM) analysis.[48,96–99] Finally, we could also generalize our proposed method to accommodate non-exponential lifetime decays if such decay probabilities are warranted by the data by modifying Eq. 5.

These, and further generalizations that can be implemented within a BNP framework, highlight the flexibility afforded by BNPs and the nature of what can be teased out from challenging data sets. Indeed, BNPs themselves suggest productive paths forward to tentatively formulate inverse strategies for challenging data sets not otherwise amenable to traditional, parametric, Bayesian analysis.[100–103]

METHOD

Here, we describe the mathematical formulation of our analysis method of time-resolved pulsed excitation single photon arrival data. For clarity we focus on measurements obtained on a fluorescence setup that use a train of identical excitation pulses. Following each pulse, one of more molecules located near the illuminated region may be excited from their ground state. As the excited molecules decay back to their ground state they may emit photons and we record the detection time. Below we describe how we analyze such recorded times.

We start from single photon detection times which consist of the raw output in a time-resolved pulsed excitation single photon arrival experiment. Similarly, these are measured based on the time difference between excitation pulses, which are time stamped, and the detection time of the first photon arriving after each pulse.[18,31,104] Precisely, our raw input is $\boldsymbol{\Delta t} = (\Delta t_1, \Delta t_2, \ldots, \Delta t_K)$ where Δt_k is the time interval between the preceding pulse's time and the photon detection time of the kth detection. In the literature, each Δt_k is often termed micro-time. As, some pulses may not lead to a photon detection, in general the

micro-times in $\boldsymbol{\Delta t}$ are fewer than the total number of pulses applied during an experiment.

Model description

We assume that, once excited, each molecule remains excited for a time period that is considerably lower (typically few nanoseconds) as compared to the time between two successive pulses (typically more than four times of the longest decay time in the sample[18]). This condition allows us to consider that any photon which is detected stems from an excitation caused by the very previous pulse and not from earlier pulses. Also, as excitation pulses in time-resolved pulsed excitation single photon arrival experiments are weak,[46,81] and typically one in ≈ 100 pulses results in a photon detection,[18] we ignore, to a very good approximation, multiple photon arrivals. As the number of detected photons coming from the background is considerably lower than the number of detected photons coming from the excited molecules, typically one to ≈ 1000, we also ignore background photons. However, background photons can be dealt with straightforwardly by modifying Eq. 7 to incorporate the effect of background in the model."

To analyze the recordings $\boldsymbol{\Delta t}$, we assume that the sample contains in total M different molecular species that are characterized by different lifetimes $\tau_1, \ldots, \tau_M$. Since molecules of each species may be excited by the pulses with different probabilities (because of different fraction of molecules contributing photons from different species), we consider a probability vector $\bar{\pi} = (\pi_1, \ldots, \pi_M)$ that gathers the probabilities of each species giving rise to a photon detection. Allowing s_k to be a tag attaining integer values $1, \ldots, M$, that indicates which species triggered the kth detection, we may write

$$s_k | \bar{\pi} \sim \mathbf{Categorical}_{1:M}\left(\bar{\pi}\right). \tag{3}$$

The above equation reads as follows "the tag s_k given $\bar{\pi}$ is a random variable sampled from a Categorical distribution." The Categorical distribution is the generalization of the

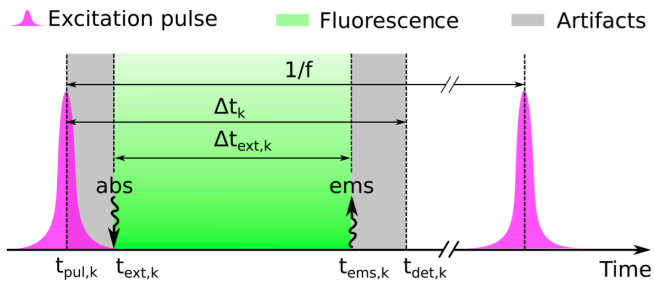

Figure 9: **Cartoon of the factors that contribute to the recorded photon arrival times.** Here, $t_{pul,k}$ is the time of the pulse's peak. Since pulses last for some time, they may excite the molecules at slightly different times. As such, we denote with $t_{ext,k}$ the absorption time of the molecule triggering the kth detection. Moreover, we denote with $t_{ems,k}$ the emission time of the photon triggering the kth detection. At last, on account of electronics limitations, the detection time, which we denote with $t_{det,k}$, might be different from $t_{ems,k}$. Here, the artifacts shown in gray originate from two sources: the left gray-shaded region is due to the width of the pulse which leads to variation in the time of the molecular excitation, and the right gray-shaded region arises from the camera-dependent detection uncertainty. The time during which the fluorophore is excited (fluorescence lifetime) is shown in green.

Bernoulli distribution which allows for more than two outcomes.[105–107] With this convention, the lifetime of the molecule triggering the kth detection is τ_{s_k}. Of course, the number of molecular species M and the precise values of the lifetimes $\tau_1, \ldots, \tau_M$ are unknown and our main task is to estimate them using the recordings in $\boldsymbol{\Delta t}$.

For clarity, we denote with $t_{pul,k}$ the application time of the pulse that triggers the kth photon detection. More precisely, $t_{pul,k}$ is the time of the pulse's peak. Because, in general pulses last for some non-zero duration, and so they may excite the molecules at slightly different times, we denote with $t_{ext,k}$ the absorption time of the molecule triggering the kth detection. Further, we denote with $t_{ems,k}$ the emission time of the photon triggering the kth detection. Finally, due to the measuring electronics, the detection time, which we denote with $t_{det,k}$, might be different from $t_{ems,k}$; see Fig. 9 for more details.

With this convention, our measured output consists of the time lags $\Delta t_k = t_{det,k} - t_{pul,k}$.

These time lags include: (i) the time until absorption occurs, $t_{ext,k} - t_{pul,k}$; (ii) the time until fluorescence emission occurs, $t_{ems,k} - t_{ext,k}$; (iii) delays and errors introduced by the measuring electronic devices, $t_{det,k} - t_{ems,k}$. Below, we denote the middle period with $\Delta t_{ext,k} = t_{ems,k} - t_{ext,k}$; while, we denote with $\Delta t_{err,k} = (t_{ext,k} - t_{pul,k}) + (t_{det,k} - t_{ems,k})$ the sum of the others. From these two, $\Delta t_{ext,k}$ is the time the molecule spends in the excited state; while, $\Delta t_{err,k}$ gathers any artifacts caused by our setup either in the excitation or detection pathway. The advantages of considering these two periods separately, as we explain below, is that (i) these represent independent physical processes, and (ii) each one is theoretically and experimentally characterized well.[18]

In particular, $\Delta t_{err,k}$ is characterized by the instrument response function (IRF) that, in each set-up, is readily obtained with calibration measurements.[18] In this study, we approximate the IRF as a Gaussian

$$\Delta t_{err,k} \sim \mathbf{Normal}(\tau_{\mathrm{IRF}}, \sigma^2_{\mathrm{IRF}}). \tag{4}$$

In this approximation, τ_{IRF} is the IRF's peak time and $\sigma_{\mathrm{IRF}} = \mathrm{FWHM}/2.355$ where FWHM is the IRF's full-width-at-half-maximum. In the Supplementary Information, we explain the IRF's calibration in detail.

Upon excitation, the time the molecule remains excited, $\Delta t_{ext,k}$, is memoryless,[18] and so it follows the exponential distribution. Therefore,

$$\Delta t_{ext,k} | \lambda_{s_k} \sim \mathbf{Exponential}(\lambda_{s_k}) \tag{5}$$

where λ_{s_k} is the inverse lifetime of the molecule triggering the detection of $\Delta t_{ext,k}$. Of course, the inverse lifetime depends upon the lifetime by $\lambda_{s_k} = 1/\tau_{s_k}$.

Because $\Delta t_{ext,k}$ and $\Delta t_{err,k}$ are independent variables, the statistics of our measurements,

which are given by $\Delta t_k = \Delta t_{ext,k} + \Delta t_{err,k}$, follow

$$\Delta t_k | \lambda_{s_k} \sim \mathbf{Normal}(\tau_{\mathrm{IRF}}, \sigma^2_{\mathrm{IRF}}) * \mathbf{Exponential}(\lambda_{s_k}) \tag{6}$$

where $*$ denotes a convolution,[108] and specifically has the probability density

$$p\left(\Delta t_k | \lambda_{s_k}\right) = \frac{\lambda_{s_k}}{2} \exp\left[\frac{\lambda_{s_k}}{2}\left(2\left(\tau_{\mathrm{IRF}} - \Delta t_k\right) + \lambda_{s_k}\sigma^2_{\mathrm{IRF}}\right)\right] \mathrm{erfc}\left(\frac{\tau_{\mathrm{IRF}} - \Delta t_k + \lambda_{s_k}\sigma^2_{\mathrm{IRF}}}{\sigma_{\mathrm{IRF}}\sqrt{2}}\right) \tag{7}$$

where $\mathrm{erfc}(\cdot)$ denotes the complementary error function. In the Supplementary Information, we show analytically how Eq. (7) arises from Eqs. (4) and (5).

In the next section we describe how Eqs. (3) and (7) can be used in conjunction with BNP to obtain the estimates we are after.

Model inference

All quantities which we wish to infer, for example the species inverse lifetimes $\lambda_1, \ldots, \lambda_M$ and excitation probabilities in $\bar{\pi}$, are represented by model variables in the preceding formulation. We infer values for these variables within the Bayesian paradigm.[75,77,79] Accordingly, on the inverse lifetimes we place independent priors

$$\lambda_m \sim \mathbf{Gamma}\left(\alpha_\lambda, \beta_\lambda\right), \qquad m = 1, \ldots, M \tag{8}$$

that ensure strictly positive values. Here, for convenience only, we consider priors on inverse lifetimes where $\tau_m = \frac{1}{\lambda_m}$ is the molecular lifetime and λ_m is the inverse lifetime of species m. As the total number of species contributing photon detections in an experiment is unknown, we consider a symmetric Dirichlet prior[75,78] (which is conjugate to the Categorical) on $\bar{\pi}$ of the form

$$\bar{\pi} \sim \mathbf{Dirichlet}_M\left(\frac{\alpha}{M}, \ldots, \frac{\alpha}{M}\right) \tag{9}$$

where α is a positive scalar hyper-parameter. A graphical summary of the whole formulation is shown on Fig. 10.

The distribution in Eq. (9) ensures that $\bar{\pi}$ are valid probability vectors. Further, Eq. (9) is specifically chosen to allow for a large, $M \to \infty$, number of species. This is particularly important because the total number of molecular species contributing to the detections in TCSPC or FLIM experiments are typically unknown, and so choosing a finite M may lead to under-fitting. Specifically, at the limiting case $M \to \infty$, the prior on Eq. (9), combined with Eq. (3), results in a Dirichlet process.[65,78,109,110] In other words, provided M is sufficiently large, the estimates obtained through our model are independent of the particular value chosen (i.e., overfitting cannot occur).

With the nonparametric model just presented, although the total number of model molecular species is infinite, the actual number of molecular species contributing photons to the measurements is finite. Specifically, the number of contributing species coincides with the number of different tags s_k associated with $\boldsymbol{\Delta t}$. In other words, instead of asking *how many species contribute to the measurements?*, with our model, we ask *how many of the represented species actually contribute at least one photon?* Further, instead of asking *what are the lifetimes of these species?* we ask *what are the lifetimes of the species contributing at least one photon?* Of course, as we estimate inverse lifetimes instead of lifetimes, we obtain the latter by $\tau_m = 1/\lambda_m$.

With these priors, we form $p\left(\bar{\pi}, s_1, \ldots, s_K, \lambda_1, \lambda_2, \ldots | \boldsymbol{\Delta t}\right)$ which is the joint posterior probability distribution that includes all unknown variables. To compute this posterior, we develop a Markov Chain Monte Carlo (MCMC) scheme[79,111] that generates pseudo-random samples with the appropriate statistics. The scheme is described in the Supplementary Information and a working implementation is also provided.

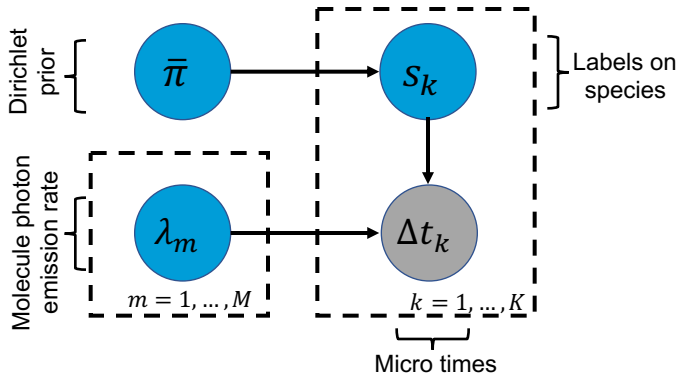

Figure 10: **Graphical representation of the proposed model**. A simple graphical representation of the model, where Δt_k is the micro time k with $k = 1, \ldots, K$. The inverse lifetime of species m is shown by λ_m, $m = 1, \ldots, M$. The label s_k tells us which of the species is contributing the kth photon. In the graphical model, the measured data are denoted by grey shaded circles and the model variables, which require priors, are designated by blue circles. Each one of the labels has a prior which is a Dirichlet probability $\overline{\pi}$.

Acquisition of Synthetic Data

The synthetic data presented in this study are obtained by standard pseudo-random computer simulations[112–116] that simulate a common fluorescence lifetime imaging modality with a conventional single-spot confocal setup. Further, in the simulations we consider confocal regions created with pulsed excitation. To generate data mimicking as closely as possible the measurements obtained in real experiments, we simulate freely diffusing molecules of different species characterized by different diffusion coefficients and lifetimes. Details and parameter choices are provide in the Supplementary Information, Tables S2 and S3.

Acquisition of Experiment Data

The synthetic data presented in this study are obtained as described below.

Sample preparation

Sample solutions of Rhodamine B (Rhod-B, Wako Pure Chemical Industries), Rhodamine 6G (Rhod-6G, Sigma-Aldrich), and tetramethylrhodamine-5-maleimide (TMR, Invitrogen), and Cy3 monofunctional NHS-ester (Cy3, GE Healthcare) were prepared with Milli-Q water at 1 μM concentration. Nonionic surfactant (0.01% Triton X-100) and 2 mM Trolox were added to prevent adsorption of dye molecules to the glass surface and reduce photophysical artifacts, respectively.

Experiments

Fluorescence lifetime measurements were carried out using a confocal fluorescence microscope with super continuum laser (Fianium SC-400-4, frequency of 40 MHz). The output of the laser was filtered by a bandpass filter (Chroma Technology D525/30 m), and focused onto the sample solution using a 60× objective lens (Nikon Plan Apo IR) with NA of 1.27. The excitation power was set to be 0.3 μW at the entrance port of the microscope. Fluorescence photons ware collected by the same objective lens and guided through a confocal pinhole as well as a bandpass filter (Chroma Technology D585/40 m), and then detected by a hybrid detector (Becker & Hickl HPM-100-40-C). For each photon signal detected, the routing information was appended by a router (Becker & Hickl HRT-82). The arrival time of the photon was measured by a TCSPC module (Becker & Hickl SPC-140) with the time-tagging mode.[45] The time resolution was evaluated by detecting the scattering of the incident laser light at a cover glass, and it was typically 180 ps at full width half maximum.

ACKNOWLEDGEMENTS

S.P. acknowledges support from the NIH NIGMS; R01GM134426 “Theoretical models of single molecule dynamics from minimal photon numbers” for the contributions and support of S.J. and R01GM130745 “A Bayesian nonparametric approach to superresolved tracking of

multiple molecules" for the contributions and support from I.S. T.T. acknowledges support from JSPS KAKENHI Grant Number JP19F19340.

AUTHOR CONTRIBUTIONS

MT and SJ analyzed data and developed analysis software; MT, SJ, IS developed computational tools; WH, KI, TT contributed experimental data; MT, SJ, IS, SP conceived research; SP oversaw all aspects of the projects.

SUPPLEMENTARY INFORMATION

In this supplement, we present additional analyses and technical details expanding upon the material presented in the main text. These include: (i) additional analysis of synthetic and experimental traces that include the estimation of lifetimes and the fraction of different species contributing photons; (ii) additional details on the theoretical approaches used; and (iii) a complete description of the inference framework developed that includes choices for prior probability distributions and a computational implementation. Moreover, in our BNP analysis, we do not pre-specify the number of species, we learn them.

Additional results

Analysis of additional synthetic data

In the main text we focused on the estimation of: lifetime, τ, with values less than 10 ns which are typical lifetime values in *in vivo* applications.[94] Here, we explore broader parameter ranges from freely diffusive molecules, Figs. S1 and S2 to the case when we have different background photons, Fig. S3, which we evaluated our method respect to different background levels to see how it behaves with different number background photons. Moreover, we evaluated our method for cases with more than two species, Figs. S4 and S5, and estimate the fraction of molecules contributing photons from different species, Fig. S6, that we explain in the main text in Section "Mixtures of different species contributing photons" .

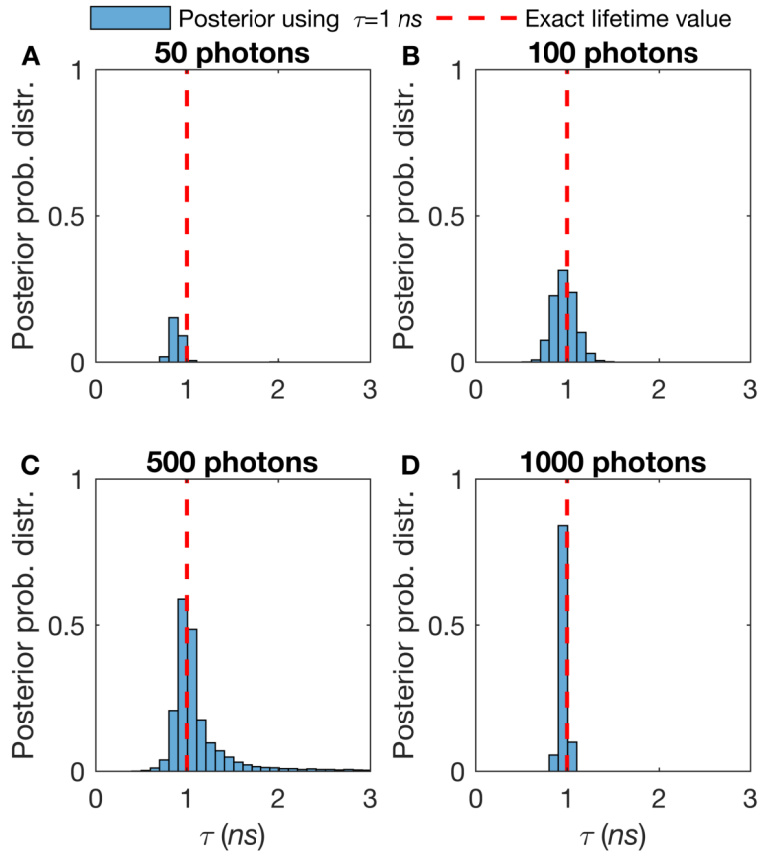

Figure S1: **Effect of the number of detected photons on a single diffusive molecular lifetime estimate. The more photons per unit time, the sharper the lifetime estimate.** Here, we work on single species lifetime while all molecules are diffusing with diffusion coefficient, $D = 10\ \mu m^2/s$. The synthetic trace is generated using $\tau = 1\ ns$. We start with 50 photons (A) and gradually increase the number of photons that we incorporate into the analysis to 100 (B), 500 (C), and 1000 (D) photons. The excitation pulses occur at a frequency of 40 MHz and we assume that these pulses assume a Gaussian shape with standard deviation of 0.1 ns. The ground truth for the lifetimes are known (as this is synthetic data) and they are shown by red-dashed lines.

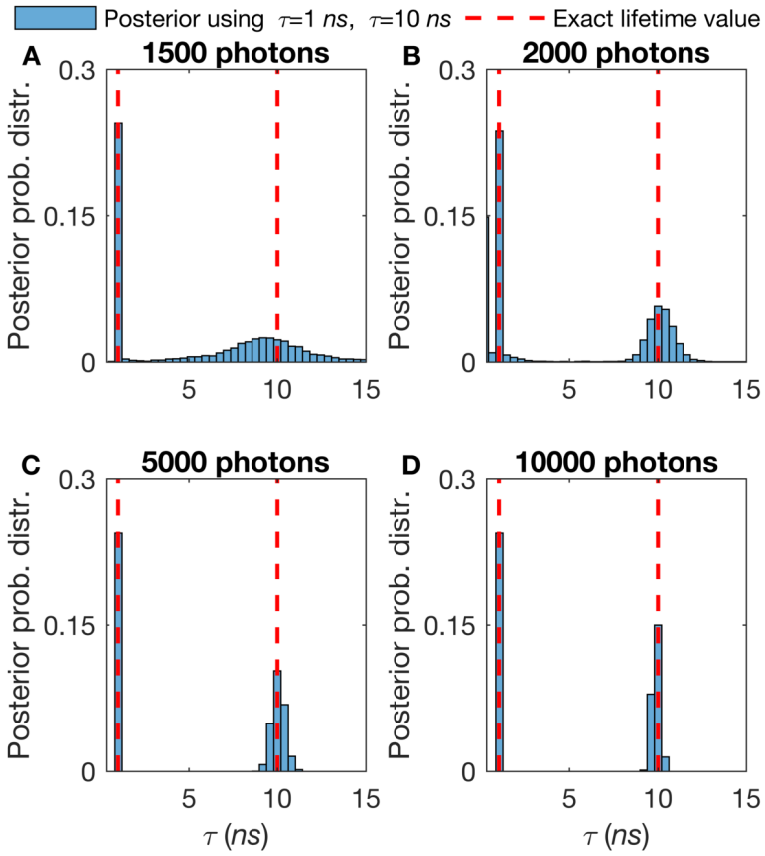

Figure S2: **Effect of the number of detected photons on a double diffusive molecular lifetime estimation. The more photons per unit time and thus the sharper estimation of lifetime.** Here, we work on single species lifetime while all molecules are diffusing with diffusion coefficient, $D = 10\ \mu m^2/s$. The synthetic trace generated by $\tau = 1\ ns$ and $\tau = 10\ ns$. We start with 1500 photons (A) and gradually increase the number of photons that we incorporate into the analysis to 2000 (B), 5000 (C), and 10000 (D) photons. Here, all other features such as the frequency of acquisition and width of pulse are the same as in Fig. S1. Also, we follow the same red-dashed line convention as in 3.

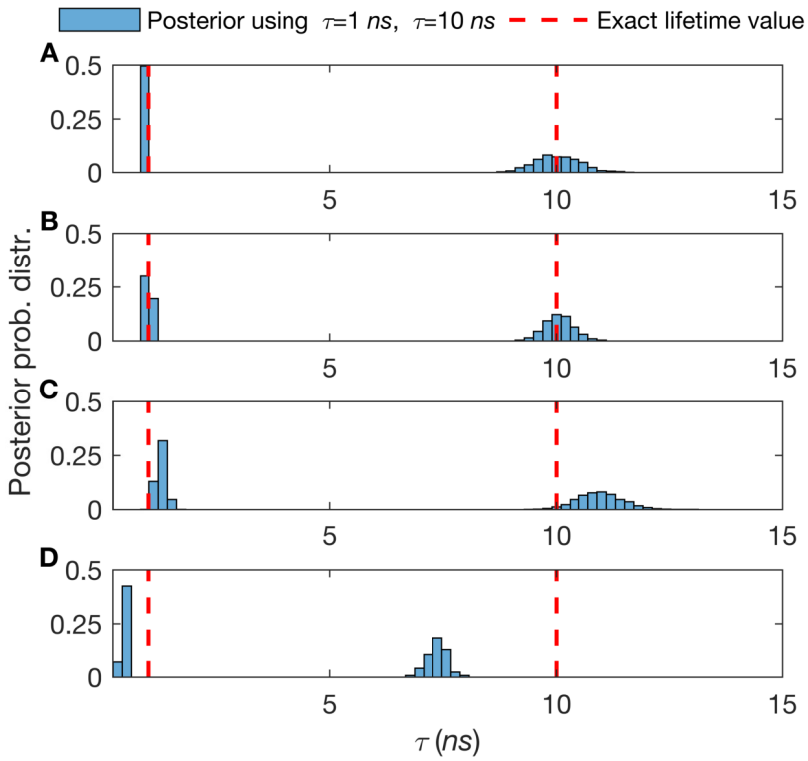

Figure S3: **Effect of the number of background photons on a double diffusive molecular lifetimes estimation. The more background photons per unit time, the poorer the lifetime estimate.** Here, we work on double species lifetime while all molecules are diffusing with diffusion coefficient, $D = 10\ \mu m^2/s$. The synthetic trace generated by $\tau = 1\ ns$ and $\tau = 10\ ns$ with total 3000 photons. We start with 3 background photons (A) and gradually increase the number of photons that we incorporate into the analysis to 30 (B), 150 (C), and 300 (D) photons. Here, all other features such as the frequency of acquisition and width of pulse are the same as in Fig. S1. Also, we follow the same red-dashed line convention as in 3.

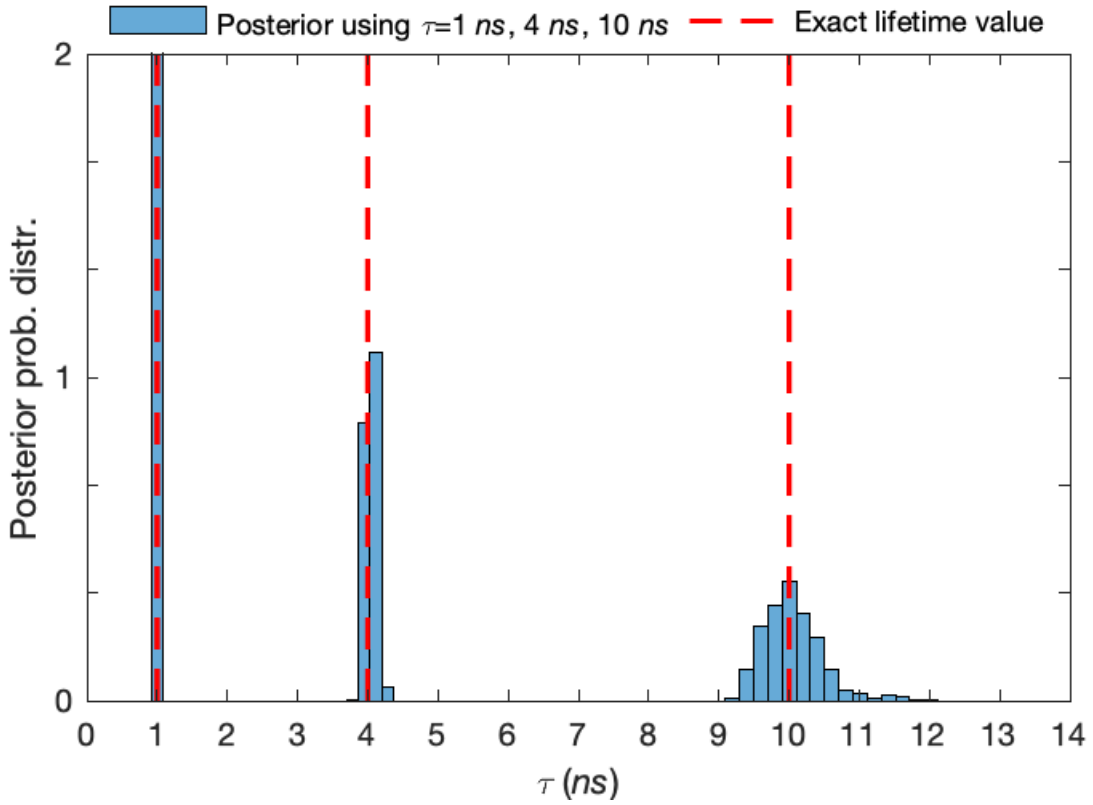

Figure S4: **Lifetime estimates with three different species using synthetic data.** Here, we generate a synthetic trace with three species having lifetimes $\tau = 1\ ns$, $\tau = 4\ ns$ and $\tau = 10\ ns$ with equal fraction of molecules contributing photons from different species (33% for each of them) and analyze a total of 2×10^5 photon arrivals. Here, all other features such as the frequency of acquisition and width of pulse are the same as in Fig. S1. Also, we follow the same red-dashed line convention as in 3.

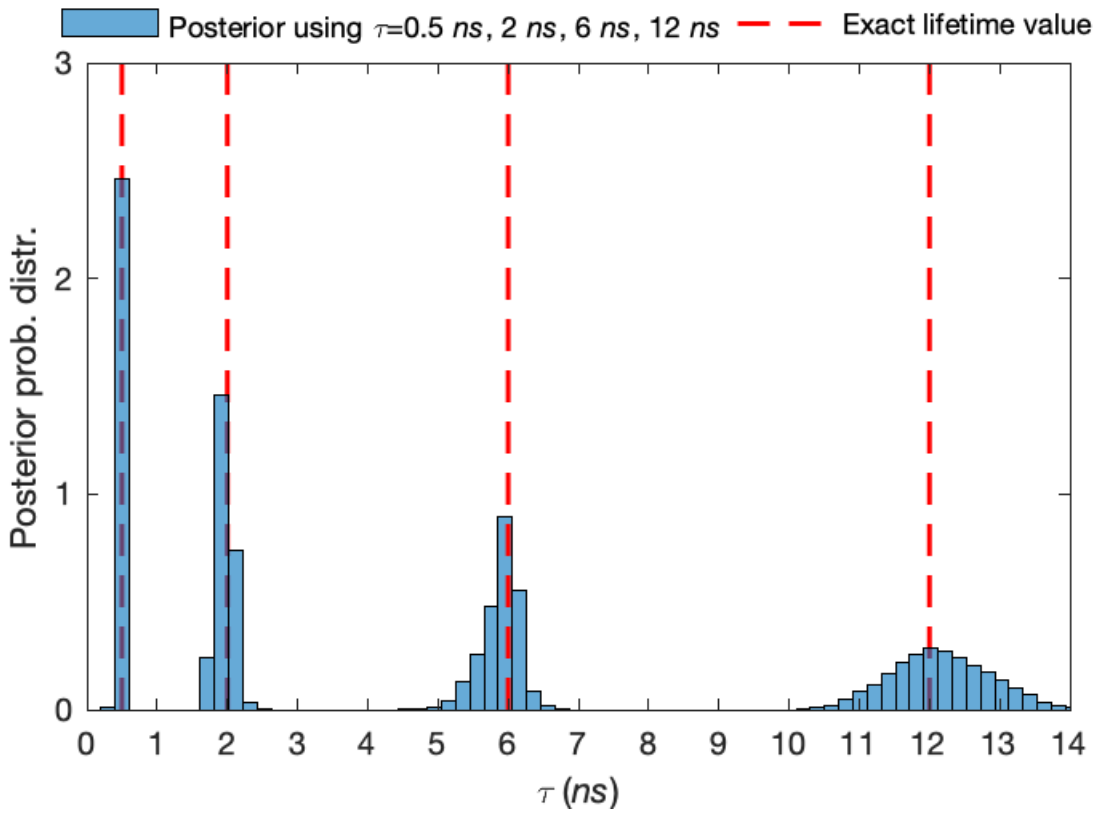

Figure S5: **Lifetime estimates with four different species in synthetic data.** Here, we work with four species lifetimes while all molecules are immobilized. The synthetic trace generated by $\tau = 0.5\ ns$, $\tau = 2\ ns$, $\tau = 6\ ns$ and $\tau = 12\ ns$ with equal fraction of molecules of each species (i.e., set at 25%) for each of them and analyze a total of 3×10^5 photon arrivals. Here, all other features such as the frequency of acquisition and width of pulse are the same as in Fig. S1. Also, we follow the same red-dashed line convention as in 3.

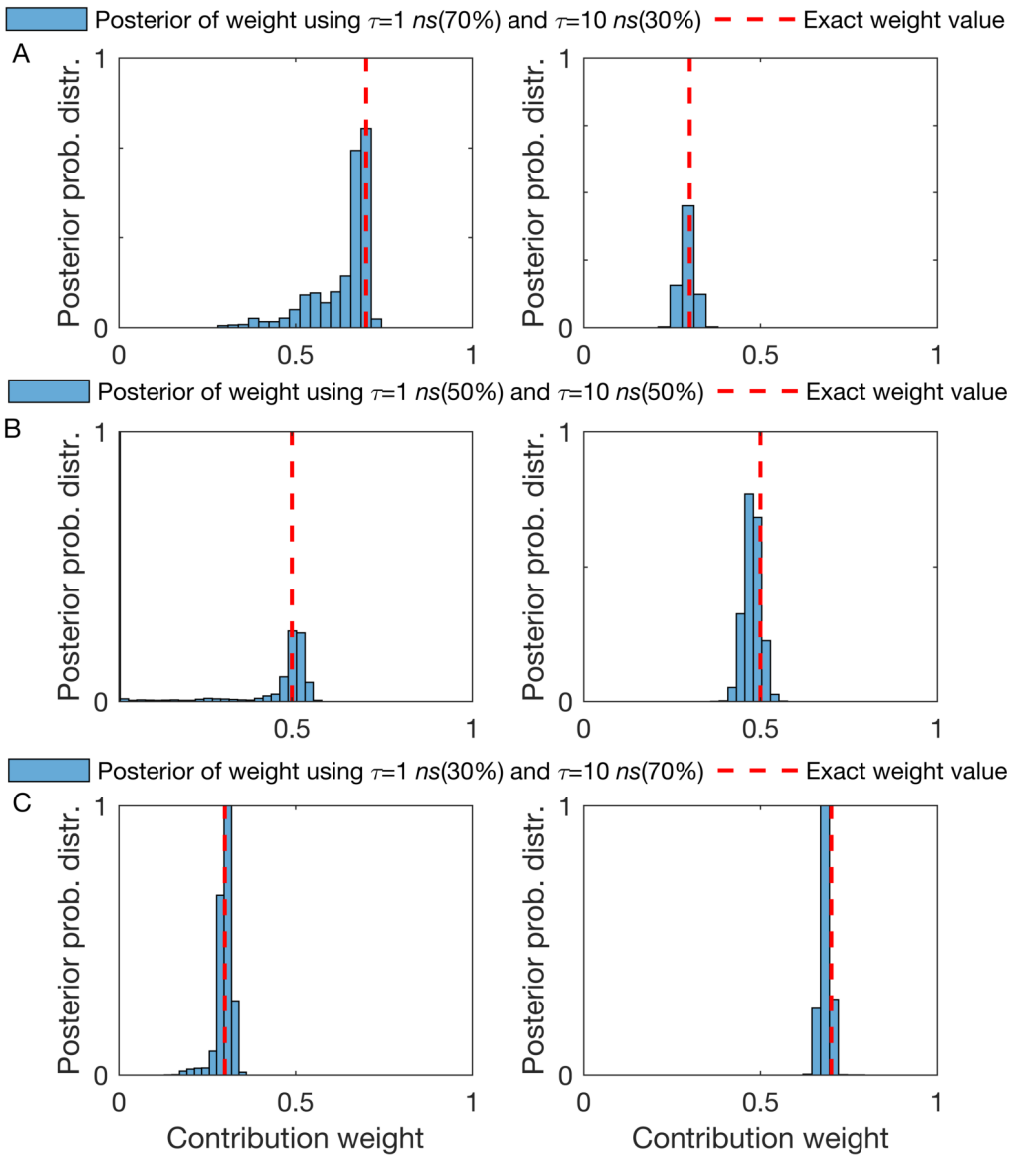

Figure S6: **Estimation of the fraction of molecules contributing photons from different species**. (A-C) Using the same synthetic traces as in Fig. 5, the posterior probability distribution over the fraction of molecules contributing photons from different species (weight) with lifetimes of 1 ns and 10 ns, 3000 total number of detected photons analyzed and fractions of chemical species of $70\% - 30\%$, $50\% - 50\%$ and $30\% - 70\%$ respectively. Here, all other features such as the frequency of acquisition and width of pulse are the same as in Fig. S1. Also, we follow the same red-dashed line convention as in 3.

Analysis of additional experimental data

Here, we used real measurements, obtained as explained in the method section, from different fluorescent dyes, namely Cy3, TMR, Rhod-B, and Rhod-6G. In Fig. S7 we considered a mixture of all four species. In Fig. S8 we show that we can correctly identify the fraction of molecules contributing photons from different species.

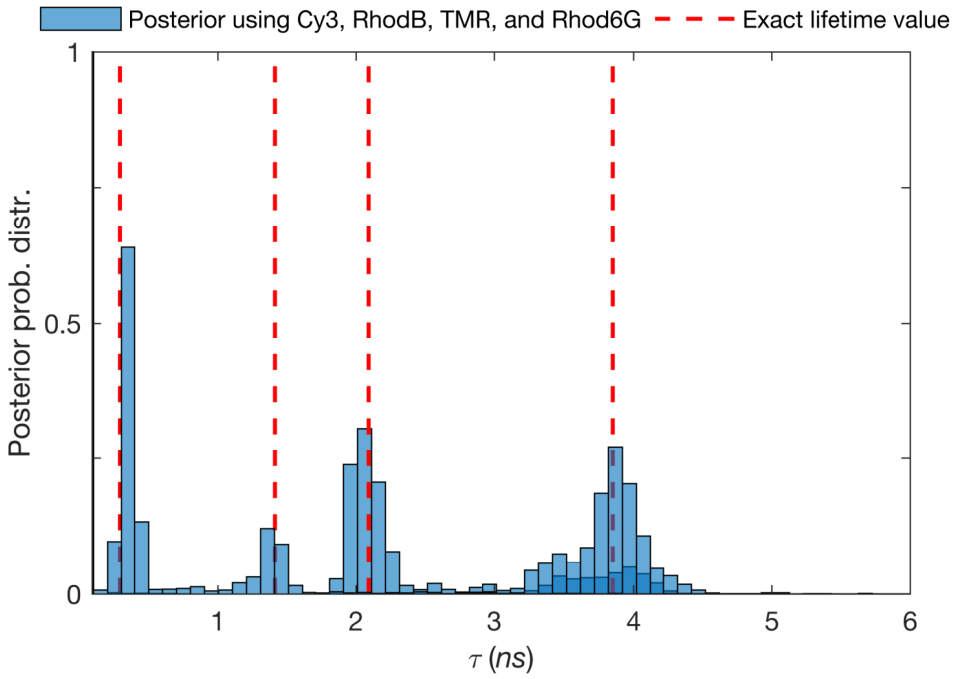

Figure S7: **Lifetime estimates for the case of four different species from experimental data.** Here, we work on four species lifetimes while all molecules are immobilized. The experimental trace generated by four different dyes including Cy3, Rhod-B, TMR, and Rhod-6G with a total of $\approx 3\times10^5$ photon arrivals analyzed. The excitation pulses occur with a frequency of 40 MHz and we assume that these pulses are modeled by a Gaussian with a standard deviation of 0.1 ns. The ground truth estimates for the lifetimes are determined using the whole trace which includes total 1.4×10^6 photon arrivals and they are shown by red-dashed lines.

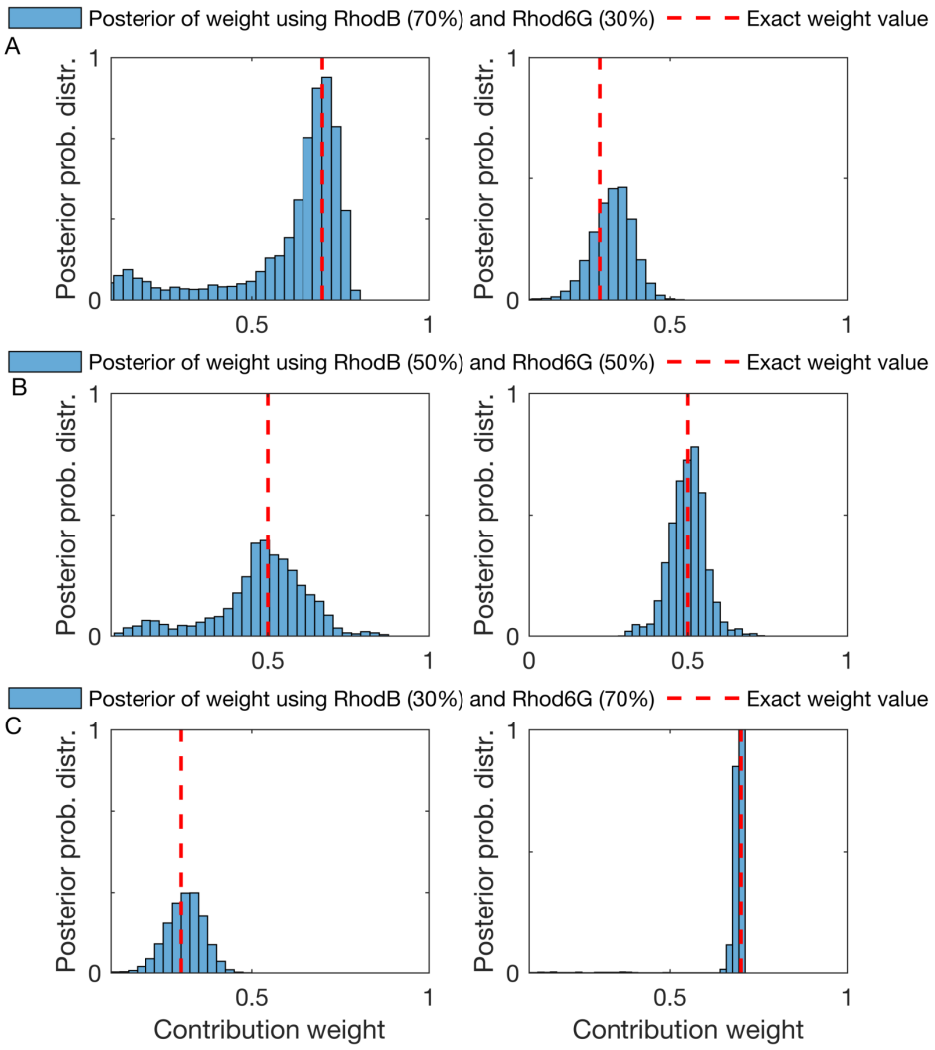

Figure S8: **Estimation of the different fraction of molecules contributing photons from different species from experimental data**. (A-C) Using the same traces as Fig. 8, the posterior probability distributions for the fraction of chemical species contributing photons for experimental dyes, RhodB and Rhod6G, with a total of ≈ 3000 total number of detected photons and fraction of chemical species contributing photons of $70\% - 30\%$, $50\% - 50\%$ and $30\% - 70\%$ respectively. The excitation pulses happen at a frequency of 40 MHz and we consider them to have a Gaussian shape with a standard deviation of 0.1 ns. What we treat as ground truth lifetime estimates (as we do not have real ground truths for experimental data) are determined using the whole trace which includes a total of 1.4×10^6 photon arrivals and they are shown by red-dashed lines.

Brief description of TCSPC and phasor plots analysis

Time domain

In typical time-domain lifetime imaging, a pulsed laser is used to excite the sample periodically, causing fluorescence emission for those pulses where a molecule is excited and decays back to the ground state radiatively. Experimentally, based on the data we presented in Fig. S9, this is typically 1 in 40 pulses.[18]

From Eq. 1, fluorescence species with M different lifetimes have exponentially decaying intensities

$$I(t) = \sum_{m=1}^{M} a_m \exp\left(-\frac{t}{\tau_m}\right) \tag{S10}$$

with fluorescence lifetimes τ_m and weights, a_m. In an ideal scenario, a fluorophore is excited with a Dirac-shaped laser pulse at time $t = 0$. Its initial intensity is therefore $I(t < 0) = 0$. As excitation pulses are not infinitely sharp and detectors exhibit delays, the recorded signal, $\hat{I}(t)$, is the convolution of its fluorescence intensity $I(t)$ with the instrumental response function (IRF);[117,118] see Eq. S21.

Frequency Domain

Frequency-domain experiments constitute an alternative way to measure excited state lifetimes. In this case, the sample is excited with an intensity-modulated light, typically a sine-wave.[18] When a fluorescent sample is excited in this way, the emission intensity follows a shifted modulation (m) pattern with the phase shift (ϕ) and peak height that both encode information on the excited state lifetime.[18]

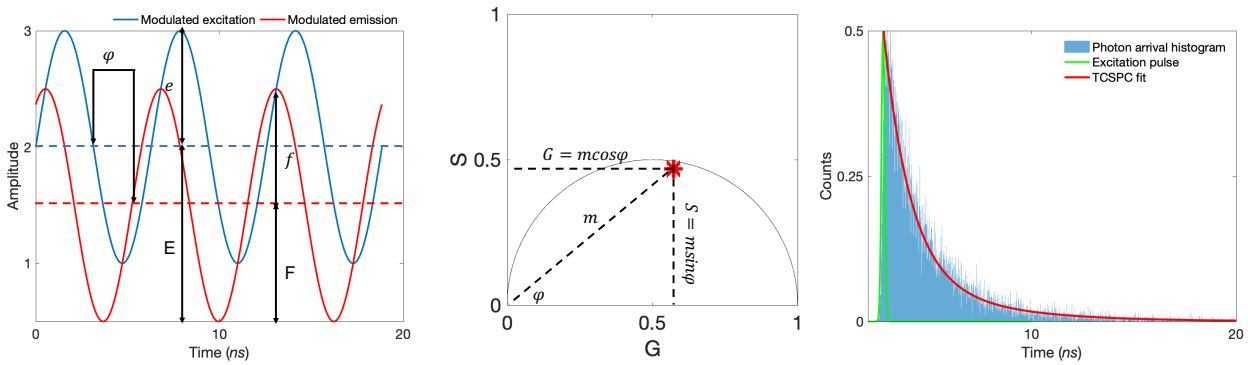

Figure S9: **Comparison between time-domain and frequency-domain analysis.** Mapping frequency-domain (left) and TCSPC (right) data to the phasor plot (middle).

The modulation of the excitation is given by $\frac{e}{E}$, where e is the average intensity and E is the peak-to-peak height of the incident light (Fig. S9). The modulation of the emission is defined similarly, $\frac{f}{F}$, except using the intensities of the emission (Fig. S9). The shifted modulation between emission and excitation, $m = (f/F)/(e/E)$. The other experimental observable is the phase shift, (ϕ) which is the phase difference between excitation and emission. Both phase shift (ϕ) and the shifted modulation between emission and excitation (m) can be employed to calculate the lifetime using

$$\tan\phi = \omega\tau_\phi \tag{S11}$$

$$m = \frac{1}{\sqrt{1+\omega^2\tau_m^2}}. \tag{S12}$$

These expressions can be also be used to calculate the phase (τ_ϕ) and shifted modulation (τ_m) lifetimes for the curves shown in Fig. S9. If the intensity decay is a single exponential, then Eqs. S11 and S12 yield the correct lifetime. In this case, both τ_ϕ and τ_m are equal. For more than one species, these two are not the same and details are discussed in Ref.[18]

Along these same lines, lifetimes can also be determined using a phasor approach first introduced by Jameson et al.[119]

Briefly, we introduce the pair of conjugate variables G and S (termed phase coordinates)

where

$$G = \frac{\int_0^{+\infty} I(t)\cos(\omega t)dt}{\int_0^{+\infty} I(t)dt} \tag{S13}$$

$$S = \frac{\int_0^{+\infty} I(t)\sin(\omega t)dt}{\int_0^{+\infty} I(t)dt}$$

and where $I(t)$ is the photon intensity.[49,117] In the case of single exponential $I(t) = a\exp(-\frac{t}{\tau})$, the coordinates of the phasor are given by

$$G = \frac{1}{1+(\omega\tau)^2} \tag{S14}$$
$$S = \frac{\omega\tau}{1+(\omega\tau)^2}.$$

IRF approximation

To incorporate the effect of the IRF in our analysis, we approximate the IRF with a Gaussian function;[39] see Fig. S10. Centrally symmetric pulses such as the Gaussian, are obtained from electronics as used in most modern instruments.[41] However, non-symmetrical IRFs could be handled by proper modifications to Eq. 4 in the main text.

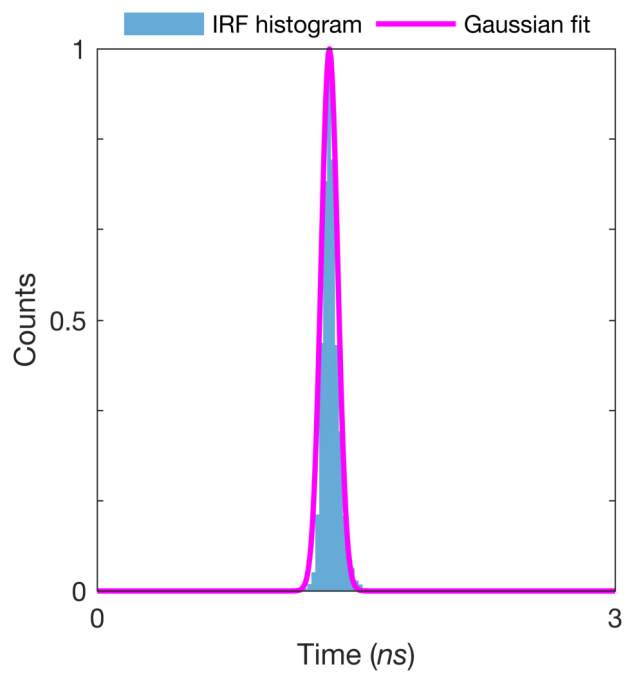

Figure S10: **The actual IRF (blue color) fitted with a Gaussian function (magenta color).** The fitted IRF is used for the analysis of all experimental data.

Description of the pulsed excitation and microtimes simulation

To simulate experimentally realistic microtimes, for mobile particles, we simulate diffusive molecules which freely traverse through an illuminated confocal volume. We define periodic boundaries ($\pm L_x$, $\pm L_y$, $\pm L_z$) which are much larger than the confocal radii to maintain a constant concentration of molecules. The confocal volume itself is pulsed on and off and the probability of excitation of a molecule depends on its location within that volume during the pulse. Here we consider the confocal volume (the combined excitation and emission point spread function, PSF) to be a 3D Gaussian, with radii of $\omega_x = 0.3$ μm, $\omega_y = 0.3$ μm, $\omega_z = 3.5$ μm and centered at the point of origin. The precise formula for this PSF is

$$\mathbf{PSF}\,(x, y, z) = \exp\left(-2\left(\left(\frac{x}{\omega_x}\right)^2 + \left(\frac{y}{\omega_y}\right)^2 + \left(\frac{z}{\omega_z}\right)^2\right)\right). \tag{S15}$$

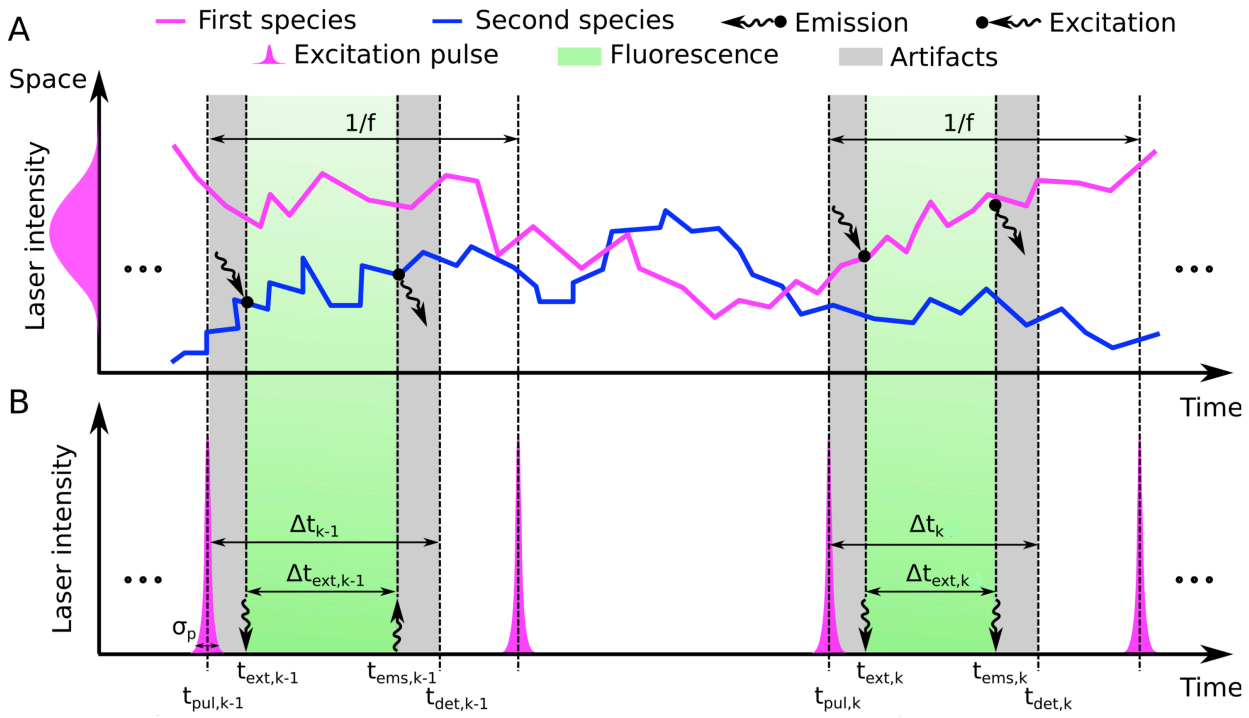

Figure S11: **Pictorial representation of the experimental setup a sample with a mixture of two species.** (A) The Brownian motion of two species in space versus time. Excitation and emission points are shown with different arrows. (B) Micro-times are the time between the peak of the pulse $t_{pul,k}$ that trigger the kth photon detection and detection time $t_{det,k}$. The time between the excitation $t_{ext,k}$ and emission $t_{ems,k}$ of the molecule, $\Delta t_{ext,k}$ follows the molecular lifetime. The gray and green-shaded regions are described in Fig. 9.

So, the emission that received by molecule n of the mth is species

$$\mu_{m,n} = \mu_{m,ext}\mathbf{PSF}\left(x, y, z\right) \tag{S16}$$

where, $\mu_{m,ext}$ is the maximum excitation rate of the molecule n of species m which occurs when the molecule is at the center of the confocal volume.[120]

Assuming that molecules do not move significantly over the duration of the pulse (of typical width 0.1 ns[121]), the probability of excitation of molecule n of species m is $q_{m,n} = \mu_{m,n}\delta t_p$ where, δt_p is the duration of the pulse. So, for any pulse excitation, we need to determine if the nth molecule of species m is excited or not. We define the variable $b_{m,n}$ to be either 1 or 0 if the molecule emits or does not emit a photon and consider this variable to be Bernoulli distributed

$$b_{m,n} \sim \mathbf{Bernoulli}\left(q_{m,n}\right). \tag{S17}$$

At the end, when a molecule is excited by each pulse $b_{m,n} = 1$, we need to consider the delays and errors introduced by the measuring electronic devices, $t_{det,k} - t_{ems,k}$. Since, we consider these errors follow a normal distribution, and the excitation time is normal distributed as well, we denote both effects with $\Delta t_{err,k} = (t_{ext,k} - t_{pul,k}) + (t_{det,k} - t_{ems,k})$ and as the result, we sample it from a normal distribution

$$\Delta t_{err,k} \sim \mathbf{Normal}(\tau_{IRF}, \sigma_{IRF}^2) \tag{S18}$$

where τ_{IRF} is the mean of IRF and σ_{IRF} is the standard deviation of the IRF (see Eq. 4 for comparison). In this simulation we considered $\sigma = \frac{\delta t_p}{2}$ as the width of the pulse.

After sampling the error time, we sample the emission time of each molecule from the exponential distribution with corresponding inverse lifetime belongs to species m

$$\Delta t_{ext,k}|\lambda_m \sim \mathbf{Exponential}\left(\lambda_m\right) \tag{S19}$$

and as we have shown in the Fig. S11 the detection time of each molecule will be sum of these two times

$$\Delta t_k = \Delta t_{ext,k} + \Delta t_{err,k} \tag{S20}$$

which is determined by the convolution of emission profile, Eq. S18, and excitation pulse, Eq. S19.

Derivation of model likelihood

As we mentioned in the main text, Section "Model description" , measurements $\Delta t_k = \Delta t_{ext,k} + \Delta t_{err,k}$, follow

$$\Delta t_k | \lambda_{s_k} \sim \mathbf{Normal}(\tau_{\mathrm{IRF}}, \sigma^2_{\mathrm{IRF}}) * \mathbf{Exponential}(\lambda_{s_k}). \tag{S21}$$

In this case we have

$$\begin{aligned}
\Delta t_k | \lambda_{s_k} &\sim \int_{-\infty}^{\infty} \mathbf{Normal}(\tau_{\mathrm{IRF}}, \sigma^2_{\mathrm{IRF}}) \mathbf{Exponential}(\lambda_{s_k}) d\Delta t_{ext} \\
&= \frac{\lambda_{s_k}}{\sqrt{2\pi\sigma^2_{\mathrm{IRF}}}} \int_{-\infty}^{\infty} e^{-\frac{(\Delta t_k - \Delta t_{ext} - \tau_{\mathrm{IRF}})^2}{2\sigma^2_{\mathrm{IRF}}}} e^{\Delta t_{ext} \lambda_{s_k}} d\Delta t_{ext} \\
&= \frac{\lambda_{s_k}}{2} \exp\left[\frac{\lambda_{s_k}}{2}\left(2\left(\tau_{\mathrm{IRF}} - \Delta t_k\right) + \lambda_{s_k}\sigma^2_{\mathrm{IRF}}\right)\right] \mathrm{erfc}\left(\frac{\tau_{\mathrm{IRF}} - \Delta t_k + \lambda_{s_k}\sigma^2_{\mathrm{IRF}}}{\sigma_{\mathrm{IRF}}\sqrt{2}}\right)
\end{aligned} \tag{S22}$$

where $\mathrm{erfc}(\cdot)$ denotes the complementary error function.

Detailed description of the inference framework

Description of prior probability distributions

Within the Bayesian approach, all unknown model parameters need priors. The model parameters in our framework that require priors are: the inverse lifetimes $\{\lambda_m\}_m$; labels on each species $\overline{s}$; and probability on the labels of species $\overline{\pi}$ (fraction of molecules contributing

photons from different species). Our choices of priors are described below.

Inverse lifetimes, $\{\lambda_m\}_m$ Here we are faced with different species which have different lifetimes. For convenience, we consider inverse lifetimes instead of lifetimes, $\tau_m = \frac{1}{\lambda_m}$, where the τ_m is the molecular lifetime and λ_m is the inverse lifetime of species m.

To learn inverse lifetimes, and to guarantee that their sampled values in our formulation attain only positive values, we place a Gamma distribution prior over them as follows

$$\lambda_m \sim \mathbf{Gamma}\left(\alpha_\lambda, \beta_\lambda\right), \tag{S23}$$

where, α_λ and β_λ are prior parameters.

Weights, $\overline{\pi}$ The weight on each species comes from the Dirichlet distribution

$$\overline{\pi} \sim \mathbf{Dirichlet}_M\left(\frac{\alpha}{M}, \ldots, \frac{\alpha}{M}\right) \tag{S24}$$

where α is the scalar parameter of the Dirichlet distribution.[65,122] This prior is conjugate to the labeled species, s_k, which simplifies the computations shown below. The Dirichlet distribution is an important multivariate continuous distribution in Bayesian statistics which is a multivariate generalization of the Beta distribution and, conveniently, conjugate to the Categorical.[123]

Labels on each species, s_k

Since we have many species, we define a label for each molecule which will tell us that molecule belongs to which species

$$s_k|\overline{\pi} \sim \mathbf{Categorical}_{1:M}\left(\overline{\pi}\right) \tag{S25}$$

where $\overline{\pi} = (\pi_1, \ldots, \pi_M)$ is the weight on each species. In other words, π_m is the fraction of photons which species m contributes to the data.

Summary of model equations

For concreteness, below we summarize all equations used in our framework, including a complete list of priors.

$$\lambda_m \sim \textbf{Gamma}\left(\alpha_\lambda, \beta_\lambda\right) \tag{S26}$$

$$\overline{\pi} \sim \textbf{Dirichlet}_M\left(\frac{\alpha}{M}, \ldots, \frac{\alpha}{M}\right) \tag{S27}$$

$$s_k|\overline{\pi} \sim \textbf{Categorical}_{1:M}\left(\overline{\pi}\right) \tag{S28}$$

$$\Delta t_k|\lambda_m, s_k \sim \frac{\lambda_{s_k}}{2} \exp\left[\frac{\lambda_{s_k}}{2}\left(2\left(\tau_{\text{IRF}} - \Delta t_k\right) + \lambda_{s_k}\sigma_{\text{IRF}}^2\right)\right] \operatorname{erfc}\left(\frac{\tau_{\text{IRF}} - \Delta t_k + \lambda_{s_k}\sigma_{\text{IRF}}^2}{\sigma_{\text{IRF}}\sqrt{2}}\right) \tag{S29}$$

Inverse problem

Within the Bayesian paradigm, our goal is to sample from the following posterior probability distribution $\mathbb{P}\left(\{\lambda_m\}_m, \overline{s}, \overline{\pi}|\boldsymbol{\Delta t}\right)$. Since, it is not possible to directly compute this distribution, we will sample the random variables $\{\lambda_m\}_m$, $\overline{s}$, and $\overline{\pi}$ from their conditional distributions through a Gibbs sampling scheme.[75,76,79,111,124] Accordingly, posterior samples are generated by updating each one of the variables involved sequentially by sampling conditioned on all other variables and the measurements $\boldsymbol{\Delta t}$.

Conceptually, the steps involved in the generation of each posterior sample $(\{\lambda_m\}_m, \overline{s}, \overline{\pi})$ are:

Update the weights on each species $\overline{\pi}$

Update the labels on species $\overline{s}$

Update the inverse lifetimes $\{\lambda_m\}_m$.

Sampling of the weights $\overline{\pi}$ To update the weights of the labels on the species $\overline{s}$, we sample them from the corresponding conditional probability $\mathbb{P}\left(\overline{\pi}|\{\lambda_m\}_m, \boldsymbol{\Delta t}, \overline{s},\right)$, which simplifies to $\mathbb{P}\left(\overline{\pi}|\overline{s}\right)$.

$$
\begin{aligned}
\overline{\pi} &\sim \mathbb{P}\left(\overline{\pi}|\overline{s}\right) \propto \mathbb{P}\left(\overline{s}|\overline{\pi}\right)\mathbb{P}\left(\overline{\pi}\right) \\
&= \left[\prod_{k=1}^{K}\mathbb{P}\left(s_k|\overline{\pi}\right)\right]\mathbb{P}\left(\overline{\pi}\right) = \left[\prod_{k=1}^{K}\pi_{s_k}\right]\mathbf{Dirichlet}_M\left(\frac{\alpha}{M},\ldots,\frac{\alpha}{M}\right) \\
&= \left[\prod_{k=1}^{K}\pi_{s_k}\right]\frac{\Gamma\left(\sum_{m=1}^{M}\frac{\alpha}{M}\right)}{\sum_{m=1}^{M}\Gamma\left(\frac{\alpha}{M}\right)}\prod_{m=1}^{M}\pi_m^{\frac{\alpha}{M}-1} \\
&= \mathbf{Dirichlet}_M\left(\frac{\alpha}{M}+\sum_{k=1}^{K}\mathbb{I}(s_k=1),\ldots,\frac{\alpha}{M}+\sum_{k=1}^{K}\mathbb{I}(s_k=M)\right).
\end{aligned}
$$

Sampling of the labels $\overline{s}$ To sample the labels on species, we sample them from the conditional probability distribution $\mathbb{P}\left(s_k|\Delta t_k, \{\lambda_m\}_m, \overline{\pi}\right)$ as follows

$$
\begin{aligned}
s_k &\sim \mathbb{P}\left(s_k|\Delta t_k, \{\lambda_m\}_m, \overline{\pi}\right) \propto \mathbb{P}\left(\Delta t_k|\{\lambda_m\}_m, s_k\right)\mathbb{P}\left(s_k|\overline{\pi}\right) \\
&= \mathbf{Categorical}_{1:M}\left(\pi_1\frac{\lambda_{s_k}}{2}\exp\left[\frac{\lambda_{s_k}}{2}\left(2\left(\tau_{\mathrm{IRF}}-\Delta t_k\right)+\lambda_{s_k}\sigma_{\mathrm{IRF}}^2\right)\right]\mathrm{erfc}\left(\frac{\tau_{\mathrm{IRF}}-\Delta t_k+\lambda_{s_k}\sigma_{\mathrm{IRF}}^2}{\sigma_{\mathrm{IRF}}\sqrt{2}}\right),\right. \\
&\quad\vdots \\
&\quad\left.,\pi_M\frac{\lambda_{s_k}}{2}\exp\left[\frac{\lambda_{s_k}}{2}\left(2\left(\tau_{\mathrm{IRF}}-\Delta t_k\right)+\lambda_{s_k}\sigma_{\mathrm{IRF}}^2\right)\right]\mathrm{erfc}\left(\frac{\tau_{\mathrm{IRF}}-\Delta t_k+\lambda_{s_k}\sigma_{\mathrm{IRF}}^2}{\sigma_{\mathrm{IRF}}\sqrt{2}}\right)\right), \quad k=1,\ldots,K.
\end{aligned}
$$

Sampling the inverse lifetimes $\{\lambda_m\}_m$ To sample λ_m, we sample from the corresponding conditional probability distribution $\mathbb{P}\left(\{\lambda_m\}_m|\boldsymbol{\Delta t}, \overline{s}\right)$ as follows

$$\begin{aligned}\{\lambda_m\}_m \sim \mathbb{P}\left(\{\lambda_m\}_m|\boldsymbol{\Delta t}, \overline{s}\right) &\propto \mathbb{P}\left(\boldsymbol{\Delta t}|\{\lambda_m\}_m, \overline{s}\right)\left[\prod_{m=1}^{M}\mathbb{P}\left(\lambda_m\right)\right] \\ &= \left[\prod_{k=1}^{K}\frac{\lambda_{s_k}}{2}\exp\left[\frac{\lambda_{s_k}}{2}\left(2\left(\tau_{\mathrm{IRF}}-\Delta t_k\right)+\lambda_{s_k}\sigma_{\mathrm{IRF}}^2\right)\right]\operatorname{erfc}\left(\frac{\tau_{\mathrm{IRF}}-\Delta t_k+\lambda_{s_k}\sigma_{\mathrm{IRF}}^2}{\sigma_{\mathrm{IRF}}\sqrt{2}}\right)\right] \\ &\times\left[\prod_{m=1}^{M}\mathbf{Gamma}\left(\lambda_m;\alpha_\lambda,\beta_\lambda\right)\right].\end{aligned} \tag{S30}$$

Since, there is no closed form to sample $\{\lambda_m\}_m$, we sample it using the Metropolis algorithm with the proposal

$$\lambda_m^{\mathrm{prop}} \sim \mathbf{Gamma}\left(\alpha_{\lambda_m}^{\mathrm{prop}}, \frac{\lambda_m^{\mathrm{old}}}{\alpha_{\lambda_m}^{\mathrm{prop}}}\right), \qquad m=1,\ldots,M$$

where, the $\alpha_{\lambda_m}^{\mathrm{prop}}$ is the parameter of the proposal distributions for the inverse lifetime. Then, the acceptance ratio is equal to

$$r_\lambda = \frac{\mathbb{P}\left(\{\lambda_m^{\mathrm{prop}}\}_{\mathrm{m}}|\boldsymbol{\Delta t}, \overline{s}\right)}{\mathbb{P}\left(\{\lambda_m^{\mathrm{old}}\}_m|\boldsymbol{\Delta t}, \overline{s}\right)}\frac{\mathrm{Proposal}\left(\{\lambda_m^{\mathrm{old}}\}_m|\{\lambda_m^{\mathrm{prop}}\}_m\right)}{\mathrm{Proposal}\left(\{\lambda_m^{\mathrm{prop}}\}_m|\{\lambda_m^{\mathrm{old}}\}_m\right)}.$$

Also, to avoid numerical underflow, we work with the logarithm of the acceptance ratio

$$\begin{aligned}\log r_\lambda = &\left[\sum_{k=1}^{K}\log\left(\frac{\lambda_{s_{\mathrm{k}}}^{\mathrm{prop}}-\lambda_{s_{\mathrm{k}}}^{\mathrm{old}}}{2}\right)+\left(\Delta t_{\mathrm{k}}-\tau_{\mathrm{IRF}}\right)\left(\lambda_{s_k}^{\mathrm{old}}-\lambda_{s_k}^{\mathrm{prop}}\right)+\frac{\sigma^2}{2}\left(\lambda^{2\,\mathrm{prop}}_{s_k}-\lambda^{2\,\mathrm{old}}_{s_k}\right)\right] \\ &+\log\left(\frac{\operatorname{erfc}\left(\frac{\tau_{\mathrm{IRF}}-\Delta t_k+\lambda_{s_k}^{\mathrm{prop}}\sigma_{\mathrm{IRF}}^2}{\sigma_{\mathrm{IRF}}\sqrt{2}}\right)}{\operatorname{erfc}\left(\frac{\tau_{\mathrm{IRF}}-\Delta t_k+\lambda_{s_k}^{\mathrm{old}}\sigma_{\mathrm{IRF}}^2}{\sigma_{\mathrm{IRF}}\sqrt{2}}\right)}\right) \\ &+\left[\sum_{m=1}^{M}\left(2\alpha_{\lambda_m}^{\mathrm{prop}}-\alpha_\lambda\right)\log\left(\frac{\lambda_m^{\mathrm{old}}}{\lambda_m^{\mathrm{prop}}}\right)+\left(\frac{\lambda_m^{\mathrm{old}}-\lambda_m^{\mathrm{prop}}}{\beta_\lambda}\right)+\alpha_{\lambda_m}^{\mathrm{prop}}\left(\frac{\lambda_m^{\mathrm{prop}}}{\lambda_m^{\mathrm{old}}}-\frac{\lambda_m^{\mathrm{old}}}{\lambda_m^{\mathrm{prop}}}\right)\right].\end{aligned} \tag{S31}$$

So, at the end we will accept or reject the proposal if

$$\log r_\lambda \geq 0 \Rightarrow \lambda_m^{\text{new}} = \lambda_{\text{m}}^{\text{prop}}, \qquad m = 1, \ldots, M$$

$$\log r_\lambda < 0 \Rightarrow \lambda_m^{\text{new}} = \lambda_m^{\text{old}}, \qquad m = 1, \ldots, M$$

Label switching correction of the molecular lifetimes Label switching is a well-known feature of BNPs.[125] It arises when we are exploring complex posterior distributions by MCMC algorithms and the likelihood of the model is invariant to the relabelling of mixture components.[126] The issue of label switching appears because the likelihood is invariant under permutation of the indices. Under symmetric priors, the posteriors also reflects the likelihood's invariance with respect to index permutation. As a result, in any MCMC algorithm, labels of the components can permute multiple times between iterations of the sampler.[127,128] Concretely, here, due to exchangeability of the molecular lifetimes, at any iteration (i) of the Gibbs sampling scheme, the corresponding lifetime of the species m might switch with the molecule's lifetime of the species m'. This label switching does not affect the joint posterior over all lifetimes.

To undo such label switching, at any iteration of the Gibbs sampling we compare the sampled lifetimes $\{\tau_m^{(i)}\}_m$ and their weights $\{\pi_m^{(i)}\}_m$ with a fixed set of lifetimes $\{\tau_m^*\}_m$ and weights $\{\pi_m^*\}_m$. Based on the distances of the lifetimes at iteration (i) from the fixed set of lifetimes, which we chose, we correct for label switching. The simple choice for this distance can be the distance between the lifetimes, but, since label switching happens in the sampled lifetimes, and subsequently the weights of each molecular lifetime, the particular distance we use incorporates the emission probability and the weights of each molecular lifetime

$$d_{m,m'} = \int_0^\infty dt \; |\pi_m \mathbf{Exp}\,(t; \tau_m) - \pi_m^* \mathbf{Exp}\,(t; \tau_m^*)| \tag{S32}$$

and we solve the assignment problem is minimizing this distance over the species $\sum_{m=1}^M d_{m,m'}$. This problem and its computation can be done efficiently by applying the Hungarian algo-

rithm.[129–131]

Table S1: Probability distributions used and their densities. Here, the corresponding random variables are denoted by x.

Distribution	Notation	Probability density function	Mean	Variance
Normal	Normal(μ, σ^2)	$\frac{1}{\sqrt{2\pi\sigma^2}} e^{-\frac{(x-\mu)^2}{2\sigma^2}}$	μ	σ^2
Exponential	Exponential(μ)	$\mu e^{-\mu x}$	$\dfrac{1}{\mu}$	$\dfrac{1}{\mu^2}$
Gamma	Gamma(α, β)	$\frac{1}{\Gamma(\alpha)\beta^\alpha} x^{\alpha-1} e^{-\frac{x}{\beta}}$	$\alpha\beta$	$\alpha\beta^2$

Table S2: Here, we list point estimates of our analyses for synthetic data, which we obtain from the marginal posterior probability distributions $p(\tau|\boldsymbol{\Delta t})$. Estimates are listed according to figure.

	τ	
	mean	std
	ns	ns
Fig. 2C	0.51 , 2.19, 10.51	0.14 , 1.42 , 6.45
Fig. 2D	0.52 , 2.36 , 13. 01	0.26 , 1.65 , 12.59
Fig. 2E	0.52 , 2.51 , 9.74	0.31 , 2.33 , 15.74
Fig. 2F	0.51 , 2.10 , 11.06	0.32 , 0.65 , 6.71
Fig. 3B1	1.17	0.29
Fig. 3B2	1.03	0.23
Fig. 3B3	1.04	0.05
Fig. 3B4	1.01	0.03
Fig. 4B1	0.82 , 8.88	0.41 , 10.31
Fig. 4B2	1.10 , 10.37	0.33 , 6.31
Fig. 4B3	1.07 , 10.08	0.15 , 4.98
Fig. 4B4	1.01 , 10.1	0.05 , 5.23
Fig. 5A	0.95 , 9.21	0.21 , 8.91
Fig. 5B	1.10 , 10.13	0.35 , 7.11
Fig. 5C	1.07 , 10.08	0.15 , 10.18
Fig. 6A	1.05 , 10.12	0.14 , 3.84
Fig. 6B	1.10 , 5.11	0.25 , 3.11
Fig. 6C	0.87 , 2.18	0.98 , 2.06
Fig. 6D	1.13 , 1.48	0.26 , 0.68
Fig. S1A	0.85	0.31
Fig. S1B	1.03	0.39
Fig. S1C	0.99	0.48
Fig. S1D	1.01	0.11
Fig. S4	1.01 , 4.10 , 10.06	0.12 , 0.35 , 5.21
Fig. S5	0.51 , 1.97 , 6.16 , 12.25	0.14 , 0.55 , 3.41 , 7.43

Table S3: Here, we list point estimates of our analyses for experimental data, which we obtain from the marginal posterior probability distributions $p(\tau|\boldsymbol{\Delta t})$. Estimates are listed according to figure.

	τ	
	mean	std
	ns	ns
Fig. 1A1	3.14	2.49
Fig. 1B1	3.84	1.84
Fig. 1C1	3.85	0.37
Fig. 7A1	1.44 , 3.39	1.14 , 1.52
Fig. 7B1	1.42 , 3.86	0.46 , 1.05
Fig. 7C1	1.41 , 3.71	0.30 , 1.10
Fig. 8A1	1.44 , 3.42	0.48 , 1.62
Fig. 8B1	1.42 , 3.91	0.39 , 1.24
Fig. 8C1	1.37 , 3.75	1.12 , 1.15
Fig. S7	0.21 , 1.37 , 2.06 , 3.89	0.25 , 0.72 , 1.41 , 2.44

References

(1) Lichtman, J. W.; Conchello, J.-A. Fluorescence microscopy. *Nature Methods* **2005**, *2*, 910.

(2) Niehörster, T.; Löschberger, A.; Gregor, I.; Krämer, B.; Rahn, H.-J.; Patting, M.; Koberling, F.; Enderlein, J.; Sauer, M. Multi-target spectrally resolved fluorescence lifetime imaging microscopy. *Nature Methods* **2016**, *13*, 257.

(3) Pawley, J. *Handbook of biological confocal microscopy*; Springer Science & Business Media, 2010.

(4) Denk, W.; Strickler, J. H.; Webb, W. W. Two-photon laser scanning fluorescence microscopy. *Science* **1990**, *248*, 73–76.

(5) Rust, M. J.; Bates, M.; Zhuang, X. Sub-diffraction-limit imaging by stochastic optical reconstruction microscopy (STORM). *Nature Methods* **2006**, *3*, 793.

(6) Ghosh, A.; Karedla, N.; Thiele, J. C.; Gregor, I.; Enderlein, J. Fluorescence lifetime correlation spectroscopy: Basics and applications. *Methods* **2018**, *140*, 32–39.

(7) Hess, S. T.; Huang, S.; Heikal, A. A.; Webb, W. W. Biological and chemical applications of fluorescence correlation spectroscopy: a review. *Biochemistry* **2002**, *41*, 697–705.

(8) Redford, G. I.; Clegg, R. M. Polar plot representation for frequency-domain analysis of fluorescence lifetimes. *Journal of Fluorescence* **2005**, *15*, 805.

(9) Hess, S. T.; Webb, W. W. Focal volume optics and experimental artifacts in confocal fluorescence correlation spectroscopy. *Biophysical Journal* **2002**, *83*, 2300–2317.

(10) Jazani, S.; Sgouralis, I.; Shafraz, O. M.; Levitus, M.; Sivasankar, S.; Pressé, S. An alternative framework for fluorescence correlation spectroscopy. *Nature Communications* **2019**, *10*, 1–10.

(11) Haupts, U.; Maiti, S.; Schwille, P.; Webb, W. W. Dynamics of fluorescence fluctuations in green fluorescent protein observed by fluorescence correlation spectroscopy. *Proceedings of the National Academy of Sciences* **1998**, *95*, 13573–13578.

(12) Jazani, S.; Sgouralis, I.; Pressé, S. A method for single molecule tracking using a conventional single-focus confocal setup. *The Journal of Chemical Physics* **2019**, *150*, 114108.

(13) Bastiaens, P. I.; Squire, A. Fluorescence lifetime imaging microscopy: spatial resolution of biochemical processes in the cell. *Trends in Cell Biology* **1999**, *9*, 48–52.

(14) Duncan, R.; Bergmann, A.; Cousin, M.; Apps, D. K.; Shipston, M. J. Multidimensional time-correlated single photon counting (TCSPC) fluorescence lifetime imaging microscopy (FLIM) to detect FRET in cells. *Journal of Microscopy* **2004**, *215*, 1–12.

(15) Gratton, E.; Breusegem, S.; Sutin, J. D.; Ruan, Q.; Barry, N. P. Fluorescence lifetime imaging for the two-photon microscope: time-domain and frequency-domain methods. *Journal of Biomedical Optics* **2003**, *8*, 381–391.

(16) Michalet, X.; Weiss, S.; Jäger, M. Single-molecule fluorescence studies of protein folding and conformational dynamics. *Chemical Reviews* **2006**, *106*, 1785–1813.

(17) Becker, W.; Bergmann, A.; Biskup, C. Multispectral fluorescence lifetime imaging by TCSPC. *Microscopy Research and Technique* **2007**, *70*, 403–409.

(18) Lakowicz, J. R. *Principles of fluorescence spectroscopy*; Springer Science & Business Media, 2013.

(19) Ankri, R.; Basu, A.; Ulku, A. C.; Bruschini, C.; Charbon, E.; Weiss, S.; Michalet, X. Single-Photon, Time-Gated, Phasor-Based Fluorescence Lifetime Imaging through Highly Scattering Medium. *Acs Photonics* **2019**, *7*, 68–79.

(20) Ulku, A.; Ardelean, A.; Antolovic, M.; Weiss, S.; Charbon, E.; Bruschini, C.; Michalet, X. Wide-field time-gated SPAD imager for phasor-based FLIM applications. *Methods and Applications in Fluorescence* **2020**, *8*, 024002.

(21) Štefl, M.; James, N. G.; Ross, J. A.; Jameson, D. M. Applications of phasors to in vitro time-resolved fluorescence measurements. *Analytical Biochemistry* **2011**, *410*, 62–69.

(22) Sameni, S.; Syed, A.; Marsh, J. L.; Digman, M. A. The phasor-FLIM fingerprints reveal shifts from OXPHOS to enhanced glycolysis in Huntington Disease. *Scientific reports* **2016**, *6*, 1–8.

(23) Ma, N.; de Mochel, N. R.; Pham, P. D.; Yoo, T. Y.; Cho, K. W.; Digman, M. A. Label-free assessment of pre-implantation embryo quality by the Fluorescence Lifetime Imaging Microscopy (FLIM)-phasor approach. *Scientific Reports* **2019**, *9*, 1–13.

(24) Digman, M. A.; Dalal, R.; Horwitz, A. F.; Gratton, E. Mapping the number of molecules and brightness in the laser scanning microscope. *Biophysical Journal* **2008**, *94*, 2320–2332.

(25) Weiss, S. Fluorescence spectroscopy of single biomolecules. *Science* **1999**, *283*, 1676–1683.

(26) Clegg, R. M.; Holub, O.; Gohlke, C. *Methods in enzymology*; Elsevier, 2003; Vol. 360; pp 509–542.

(27) Sun, Y.; Day, R. N.; Periasamy, A. Investigating protein-protein interactions in living cells using fluorescence lifetime imaging microscopy. *Nature Protocols* **2011**, *6*, 1324.

(28) OLeary, M.; Boas, D.; Li, X.; Chance, B.; Yodh, A. Fluorescence lifetime imaging in turbid media. *Optics Letters* **1996**, *21*, 158–160.

(29) Orte, A.; Alvarez-Pez, J. M.; Ruedas-Rama, M. J. Fluorescence lifetime imaging microscopy for the detection of intracellular pH with quantum dot nanosensors. *ACS Nano* **2013**, *7*, 6387–6395.

(30) Datta, R.; Alfonso-García, A.; Cinco, R.; Gratton, E. Fluorescence lifetime imaging of endogenous biomarker of oxidative stress. *Scientific Reports* **2015**, *5*, 9848.

(31) van Munster, E. B.; Gadella, T. W. *Microscopy techniques*; Springer, 2005; pp 143–175.

(32) Elson, D.; Requejo-Isidro, J.; Munro, I.; Reavell, F.; Siegel, J.; Suhling, K.; Tadrous, P.; Benninger, R.; Lanigan, P.; McGinty, J. et al. Time-domain fluorescence lifetime imaging applied to biological tissue. *Photochemical & Photobiological Sciences* **2004**, *3*, 795–801.

(33) Gopich, I. V.; Szabo, A. Theory of the energy transfer efficiency and fluorescence lifetime distribution in single-molecule FRET. *Proceedings of the National Academy of Sciences* **2012**, *109*, 7747–7752.

(34) Chung, H. S.; Louis, J. M.; Gopich, I. V. Analysis of fluorescence lifetime and energy transfer efficiency in single-molecule photon trajectories of fast-folding proteins. *The Journal of Physical Chemistry B* **2016**, *120*, 680–699.

(35) Yoo, J.; Louis, J. M.; Gopich, I. V.; Chung, H. S. Three-color single-molecule FRET and fluorescence lifetime analysis of fast protein folding. *The Journal of Physical Chemistry B* **2018**, *122*, 11702–11720.

(36) Merchant, K. A.; Best, R. B.; Louis, J. M.; Gopich, I. V.; Eaton, W. A. Characterizing the unfolded states of proteins using single-molecule FRET spectroscopy and molecular simulations. *Proceedings of the National Academy of Sciences* **2007**, *104*, 1528–1533.

(37) Gregor, I.; Patting, M. *Advanced Photon Counting*; Springer, 2014; pp 241–263.

(38) Sapermsap, N.; Li, D. D.-U.; Al-Hemedawi, R.; Li, Y.; Yu, J.; Birch, D. J.; Chen, Y. A rapid analysis platform for investigating the cellular locations of bacteria using two-photon fluorescence lifetime imaging microscopy. *Methods and Applications in Fluorescence* **2020**, *8*, 034001.

(39) Rowley, M. I.; Barber, P. R.; Coolen, A. C.; Vojnovic, B. Bayesian analysis of fluorescence lifetime imaging data. Multiphoton Microscopy in the Biomedical Sciences XI. 2011; p 790325.

(40) Kaye, B.; Foster, P. J.; Yoo, T. Y.; Needleman, D. J. Developing and testing a Bayesian analysis of fluorescence lifetime measurements. *PloS One* **2017**, *12*, e0169337.

(41) Rowley, M. I.; Coolen, A. C.; Vojnovic, B.; Barber, P. R. Robust Bayesian fluorescence lifetime estimation, decay model selection and instrument response determination for low-intensity FLIM imaging. *PloS One* **2016**, *11*, e0158404.

(42) Santra, K.; Smith, E. A.; Song, X.; Petrich, J. W. A Bayesian Approach for Extracting Fluorescence Lifetimes from Sparse Data Sets and Its Significance for Imaging Experiments. *Photochemistry and Photobiology* **2019**, *95*, 773–779.

(43) Wang, S.; Chacko, J. V.; Sagar, A. K.; Eliceiri, K. W.; Yuan, M. Nonparametric empirical Bayesian framework for fluorescence-lifetime imaging microscopy. *Biomedical Optics Express* **2019**, *10*, 5497–5517.

(44) Ishii, K.; Tahara, T. Two-dimensional fluorescence lifetime correlation spectroscopy. 1. Principle. *The Journal of Physical Chemistry B* **2013**, *117*, 11414–11422.

(45) Ishii, K.; Tahara, T. Two-dimensional fluorescence lifetime correlation spectroscopy. 2. Application. *The Journal of Physical Chemistry B* **2013**, *117*, 11423–11432.

(46) Becker, W. *Advanced time-correlated single photon counting applications*; Springer, 2015; Vol. 111.

(47) Ishii, K.; Otosu, T.; Tahara, T. *Advanced Photon Counting*; Springer, 2014; pp 111–128.

(48) Verveer, P. J.; Squire, A.; Bastiaens, P. I. Global analysis of fluorescence lifetime imaging microscopy data. *Biophysical Journal* **2000**, *78*, 2127–2137.

(49) Digman, M. A.; Caiolfa, V. R.; Zamai, M.; Gratton, E. The phasor approach to fluorescence lifetime imaging analysis. *Biophysical Journal* **2008**, *94*, L14–L16.

(50) Pelet, S.; Previte, M.; Laiho, L.; So, P. A fast global fitting algorithm for fluorescence lifetime imaging microscopy based on image segmentation. *Biophysical Journal* **2004**, *87*, 2807–2817.

(51) Ranjit, S.; Datta, R.; Dvornikov, A.; Gratton, E. Multicomponent Analysis of Phasor Plot in a Single Pixel to Calculate Changes of Metabolic Trajectory in Biological Systems. *The Journal of Physical Chemistry A* **2019**, *123*, 9865–9873.

(52) Clayton, A.; Hanley, Q.; Verveer, P. Graphical representation and multicomponent analysis of single-frequency fluorescence lifetime imaging microscopy data. *Journal of Microscopy* **2004**, *213*, 1–5.

(53) Stringari, C.; Cinquin, A.; Cinquin, O.; Digman, M. A.; Donovan, P. J.; Gratton, E. Phasor approach to fluorescence lifetime microscopy distinguishes different metabolic states of germ cells in a live tissue. *Proceedings of the National Academy of Sciences* **2011**, *108*, 13582–13587.

(54) Becker, W. Fluorescence lifetime imaging–techniques and applications. *Journal of Microscopy* **2012**, *247*, 119–136.

(55) Lou, J.; Scipioni, L.; Wright, B. K.; Bartolec, T. K.; Zhang, J.; Masamsetti, V. P.; Gaus, K.; Gratton, E.; Cesare, A. J.; Hinde, E. Phasor histone FLIM-FRET microscopy quantifies spatiotemporal rearrangement of chromatin architecture during

the DNA damage response. *Proceedings of the National Academy of Sciences* **2019**, *116*, 7323–7332.

(56) Colyer, R. A.; Weiss, S.; Michalet, X.; Siegmund, O. H.; Tremsin, A. S.; Vallerga, J. Phasor imaging with a widefield photon-counting detector. *Journal of Biomedical Optics* **2012**, *17*, 016008.

(57) Fereidouni, F.; Esposito, A.; Blab, G.; Gerritsen, H. A modified phasor approach for analyzing time-gated fluorescence lifetime images. *Journal of Microscopy* **2011**, *244*, 248–258.

(58) Grecco, H. E.; Roda-Navarro, P.; Verveer, P. J. Global analysis of time correlated single photon counting FRET-FLIM data. *Optics express* **2009**, *17*, 6493–6508.

(59) Ranjit, S.; Malacrida, L.; Jameson, D. M.; Gratton, E. Fit-free analysis of fluorescence lifetime imaging data using the phasor approach. *Nature Protocols* **2018**, *13*, 1979–2004.

(60) Liang, Z.; Lou, J.; Scipioni, L.; Gratton, E.; Hinde, E. Quantifying nuclear wide chromatin compaction by phasor analysis of histone Förster resonance energy transfer (FRET) in frequency domain fluorescence lifetime imaging microscopy (FLIM) data. *Data in Brief* **2020**, 105401.

(61) Ranjit, S.; Malacrida, L.; Stakic, M.; Gratton, E. Determination of the metabolic index using the fluorescence lifetime of free and bound nicotinamide adenine dinucleotide using the phasor approach. *Journal of biophotonics* **2019**, *12*, e201900156.

(62) Hinde, E.; Digman, M. A.; Welch, C.; Hahn, K. M.; Gratton, E. Biosensor Förster resonance energy transfer detection by the phasor approach to fluorescence lifetime imaging microscopy. *Microscopy Research and Technique* **2012**, *75*, 271–281.

(63) Fereidouni, F.; Bader, A. N.; Gerritsen, H. C. Spectral phasor analysis allows rapid and reliable unmixing of fluorescence microscopy spectral images. *Optics Express* **2012**, *20*, 12729–12741.

(64) Scipioni, L.; Gratton, E.; Diaspro, A.; Lanzano, L. Phasor analysis of local ICS detects heterogeneity in size and number of intracellular vesicles. *Biophysical journal* **2016**, *111*, 619–629.

(65) Ferguson, T. S. A Bayesian analysis of some nonparametric problems. *The annals of statistics* **1973**, 209–230.

(66) Gershman, S. J.; Blei, D. M. A tutorial on Bayesian nonparametric models. *Journal of Mathematical Psychology* **2012**, *56*, 1–12.

(67) Sgouralis, I.; Madaan, S.; Djutanta, F.; Kha, R.; Hariadi, R. F.; Presse?, S. A Bayesian Nonparametric Approach to Single Molecule Fo?rster Resonance Energy Transfer. *The Journal of Physical Chemistry B* **2018**, *123*, 675–688.

(68) Sgouralis, I.; Whitmore, M.; Lapidus, L.; Comstock, M. J.; Pressé, S. Single molecule force spectroscopy at high data acquisition: A Bayesian nonparametric analysis. *The Journal of chemical physics* **2018**, *148*, 123320.

(69) Tavakoli, M.; Jazani, S.; Sgouralis, I.; Shafraz, O. M.; Sivasankar, S.; Donaphon, B.; Levitus, M.; Pressé, S. Pitching Single-Focus Confocal Data Analysis One Photon at a Time with Bayesian Nonparametrics. *Physical Review X* **2020**, *10*, 011021.

(70) Köllner, M.; Wolfrum, J. How many photons are necessary for fluorescence-lifetime measurements? *Chemical Physics Letters* **1992**, *200*, 199–204.

(71) Esposito, A.; Gerritsen, H. C.; Wouters, F. S. Optimizing frequency-domain fluorescence lifetime sensing for high-throughput applications: photon economy and acquisition speed. *JOSA A* **2007**, *24*, 3261–3273.

(72) Turgeman, L.; Fixler, D. Photon efficiency optimization in time-correlated single photon counting technique for fluorescence lifetime imaging systems. *IEEE Transactions on Biomedical Engineering* **2013**, *60*, 1571–1579.

(73) Elder, A.; Schlachter, S.; Kaminski, C. F. Theoretical investigation of the photon efficiency in frequency-domain fluorescence lifetime imaging microscopy. *JOSA A* **2008**, *25*, 452–462.

(74) Sgouralis, I.; Presse, S. Analyzing Single Molecule Measurements With Bayesian Non-Parametric Methods. *APS* **2017**, *2017*, A5–006.

(75) Tavakoli, M.; Taylor, J. N.; Li, C.-B.; Komatsuzaki, T.; Pressé, S. Single molecule data analysis: An introduction. *arXiv preprint arXiv:1606.00403* **2016**,

(76) Von Toussaint, U. Bayesian inference in physics. *Reviews of Modern Physics* **2011**, *83*, 943.

(77) Lee, A.; Tsekouras, K.; Calderon, C.; Bustamante, C.; Pressé, S. Unraveling the thousand word picture: an introduction to super-resolution data analysis. *Chemical Reviews* **2017**, *117*, 7276–7330.

(78) Sgouralis, I.; Pressé, S. An introduction to infinite HMMS for single-molecule data analysis. *Biophysical Journal* **2017**, *112*, 2021–2029.

(79) Gelman, A.; Carlin, J. B.; Stern, H. S.; Dunson, D. B.; Vehtari, A.; Rubin, D. B. *Bayesian data analysis*; CRC press Boca Raton, FL, 2014; Vol. 2.

(80) Berezin, M. Y.; Achilefu, S. Fluorescence lifetime measurements and biological imaging. *Chemical Reviews* **2010**, *110*, 2641–2684.

(81) Becker, W.; Bergmann, A.; Hink, M.; König, K.; Benndorf, K.; Biskup, C. Fluorescence lifetime imaging by time-correlated single-photon counting. *Microscopy Research and Technique* **2004**, *63*, 58–66.

(82) Magde, D.; Rojas, G. E.; Seybold, P. G. Solvent dependence of the fluorescence lifetimes of xanthene dyes. *Photochemistry and Photobiology* **1999**, *70*, 737–744.

(83) Magde, D.; Wong, R.; Seybold, P. G. Fluorescence quantum yields and their relation to lifetimes of rhodamine 6G and fluorescein in nine solvents: Improved absolute standards for quantum yields¶. *Photochemistry and photobiology* **2002**, *75*, 327–334.

(84) Boens, N.; Qin, W.; Basarić, N.; Hofkens, J.; Ameloot, M.; Pouget, J.; Lefevre, J.-P.; Valeur, B.; Gratton, E.; Vandeven, M. et al. Fluorescence lifetime standards for time and frequency domain fluorescence spectroscopy. *Analytical chemistry* **2007**, *79*, 2137–2149.

(85) Ishii, K.; Tahara, T. Resolving inhomogeneity using lifetime-weighted fluorescence correlation spectroscopy. *The Journal of Physical Chemistry B* **2010**, *114*, 12383–12391.

(86) Michalet, X.; Siegmund, O.; Vallerga, J.; Jelinsky, P.; Millaud, J.; Weiss, S. Detectors for single-molecule fluorescence imaging and spectroscopy. *Journal of Modern Optics* **2007**, *54*, 239–281.

(87) Fox, E.; Sudderth, E. B.; Jordan, M. I.; Willsky, A. S. Nonparametric Bayesian learning of switching linear dynamical systems. Advances in neural information processing systems. 2009; pp 457–464.

(88) Fox, E.; Sudderth, E. B.; Jordan, M. I.; Willsky, A. S. Bayesian nonparametric inference of switching dynamic linear models. *IEEE Transactions on Signal Processing* **2011**, *59*, 1569–1585.

(89) Orbanz, P.; Teh, Y. W. Bayesian Nonparametric Models. *Encyclopedia of Machine Learning* **2010**,

(90) Teh, Y. W.; Jordan, M. I. Hierarchical Bayesian nonparametric models with applications. *Bayesian Nonparametrics* **2010**, *1*, 158–207.

(91) Teh, Y. W. Dirichlet process. *Encyclopedia of Machine Learning* **2010**, 280–287.

(92) Sgouralis, I.; Pressé, S. ICON: an adaptation of infinite HMMs for time traces with drift. *Biophysical Journal* **2017**, *112*, 2117–2126.

(93) Basuki, J. S.; Duong, H. T.; Macmillan, A.; Erlich, R. B.; Esser, L.; Akerfeldt, M. C.; Whan, R. M.; Kavallaris, M.; Boyer, C.; Davis, T. P. Using fluorescence lifetime imaging microscopy to monitor theranostic nanoparticle uptake and intracellular doxorubicin release. *ACS nano* **2013**, *7*, 10175–10189.

(94) Sun, Y.; Phipps, J.; Elson, D. S.; Stoy, H.; Tinling, S.; Meier, J.; Poirier, B.; Chuang, F. S.; Farwell, D. G.; Marcu, L. Fluorescence lifetime imaging microscopy: in vivo application to diagnosis of oral carcinoma. *Optics Letters* **2009**, *34*, 2081–2083.

(95) Skala, M. C.; Riching, K. M.; Bird, D. K.; Gendron-Fitzpatrick, A.; Eickhoff, J.; Eliceiri, K. W.; Keely, P. J.; Ramanujam, N. In vivo multiphoton fluorescence lifetime imaging of protein-bound and free nicotinamide adenine dinucleotide in normal and precancerous epithelia. *Journal of Biomedical Optics* **2007**, *12*, 024014.

(96) Gadella Jr, T. W.; Jovin, T. M.; Clegg, R. M. Fluorescence lifetime imaging microscopy (FLIM): spatial resolution of microstructures on the nanosecond time scale. *Biophysical Chemistry* **1993**, *48*, 221–239.

(97) Colyer, R. A.; Lee, C.; Gratton, E. A novel fluorescence lifetime imaging system that optimizes photon efficiency. *Microscopy research and technique* **2008**, *71*, 201–213.

(98) Torno, K.; Wright, B. K.; Jones, M. R.; Digman, M. A.; Gratton, E.; Phillips, M. Real-time analysis of metabolic activity within Lactobacillus acidophilus by phasor

fluorescence lifetime imaging microscopy of NADH. *Current microbiology* **2013**, *66*, 365–367.

(99) Battisti, A.; Digman, M. A.; Gratton, E.; Storti, B.; Beltram, F.; Bizzarri, R. Intracellular pH measurements made simple by fluorescent protein probes and the phasor approach to fluorescence lifetime imaging. *Chemical Communications* **2012**, *48*, 5127–5129.

(100) Bryan IV, J. S.; Sgouralis, I.; Pressé, S. Inferring effective forces for Langevin dynamics using Gaussian processes. *The Journal of Chemical Physics* **2020**, *152*, 124106.

(101) Tavakoli, M.; Jazani, S.; Sgouralis, I.; Presse, S. Single Molecules Dynamics Learned from Single Photons-Flim and FCS with Bayesian Nonparametrics. *Biophysical Journal* **2020**, *118*, 313a–314a.

(102) Tavakoli, M.; Jazani, S.; Sgouralis, I.; Presse, S. Bayesian nonparametrics for fluorescence methods. *Biophysical Journal* **2019**, *116*, 39a.

(103) Kilic, Z.; Pressé, S. Bayesian nonparametric analysis of transcriptional processes. *Biophysical Journal* **2019**, *116*, 299a.

(104) O'Connor, D. *Time-correlated single photon counting*; Academic Press, 2012.

(105) Sivia, D.; Skilling, J. *Data analysis: a Bayesian tutorial*; OUP Oxford, 2006.

(106) Bishop, C. M. *Pattern recognition and machine learning*; springer, 2006.

(107) Murphy, K. P. *Machine learning: a probabilistic perspective*; MIT press, 2012.

(108) Hirschman, I. I.; Widder, D. V. *The convolution transform*; Courier Corporation, 2012.

(109) Neal, R. M. Markov chain sampling methods for Dirichlet process mixture models. *Journal of Computational and Graphical Statistics* **2000**, *9*, 249–265.

(110) Gelfand, A. E.; Kottas, A.; MacEachern, S. N. Bayesian nonparametric spatial modeling with Dirichlet process mixing. *Journal of the American Statistical Association* **2005**, *100*, 1021–1035.

(111) Robert, C.; Casella, G. *Introducing Monte Carlo Methods with R*; Springer Science & Business Media, 2009.

(112) Berg, H. C. *Random walks in biology*; Princeton University Press, 1993.

(113) Ibe, O. C. *Elements of random walk and diffusion processes*; John Wiley & Sons, 2013.

(114) Haile, J. M. *Molecular dynamics simulation: elementary methods*; Wiley New York, 1992; Vol. 1.

(115) Higham, D. J. An algorithmic introduction to numerical simulation of stochastic differential equations. *SIAM Review* **2001**, *43*, 525–546.

(116) Erban, R.; Chapman, S. J. Stochastic modelling of reaction–diffusion processes: algorithms for bimolecular reactions. *Physical Biology* **2009**, *6*, 046001.

(117) Lakner, P. H.; Monaghan, M. G.; Möller, Y.; Olayioye, M. A.; Schenke-Layland, K. Applying phasor approach analysis of multiphoton FLIM measurements to probe the metabolic activity of three-dimensional in vitro cell culture models. *Scientific reports* **2017**, *7*, 42730.

(118) Warren, S. C.; Margineanu, A.; Alibhai, D.; Kelly, D. J.; Talbot, C.; Alexandrov, Y.; Munro, I.; Katan, M.; Dunsby, C.; French, P. M. Rapid global fitting of large fluorescence lifetime imaging microscopy datasets. *PLoS One* **2013**, *8*.

(119) Jameson, D. M.; Gratton, E.; Hall, R. D. The measurement and analysis of heterogeneous emissions by multifrequency phase and modulation fluorometry. *Applied spectroscopy reviews* **1984**, *20*, 55–106.

(120) Enderlein, J.; Ambrose, W. P. Optical collection efficiency function in single-molecule detection experiments. *Applied Optics* **1997**, *36*, 5298–5302.

(121) Otosu, T.; Ishii, K.; Oikawa, H.; Arai, M.; Takahashi, S.; Tahara, T. Highly heterogeneous nature of the native and unfolded states of the B domain of protein a revealed by two-dimensional fluorescence lifetime correlation spectroscopy. *The Journal of Physical Chemistry B* **2017**, *121*, 5463–5473.

(122) Ng, K. W.; Tian, G.-L.; Tang, M.-L. *Dirichlet and related distributions: Theory, methods and applications*; John Wiley & Sons, 2011; Vol. 888.

(123) Lin, J. On the dirichlet distribution. Ph.D. thesis, Masters thesis, Department of Mathematics and Statistics, Queens University , 2016.

(124) Liu, H.; Motoda, H. *Computational methods of feature selection*; CRC Press, 2007.

(125) Jasra, A.; Holmes, C. C.; Stephens, D. A. Markov chain Monte Carlo methods and the label switching problem in Bayesian mixture modeling. *Statistical Science* **2005**, 50–67.

(126) Egidi, L.; Pappada, R.; Pauli, F.; Torelli, N. Relabelling in Bayesian mixture models by pivotal units. *Statistics and Computing* **2018**, *28*, 957–969.

(127) Stephens, M. Dealing with label switching in mixture models. *Journal of the Royal Statistical Society: Series B (Statistical Methodology)* **2000**, *62*, 795–809.

(128) Rodriguez, C. E.; Walker, S. G. Label switching in Bayesian mixture models: Deterministic relabeling strategies. *Journal of Computational and Graphical Statistics* **2014**, *23*, 25–45.

(129) Mills-Tettey, G. A.; Stentz, A.; Dias, M. B. The dynamic hungarian algorithm for the assignment problem with changing costs. **2007**,

(130) Kuhn, H. W. The Hungarian method for the assignment problem. *Naval Research Logistics Quarterly* **1955**, *2*, 83–97.

(131) Munkres, J. Algorithms for the assignment and transportation problems. *Journal of the Society for Industrial and Applied Mathematics* **1957**, *5*, 32–38.
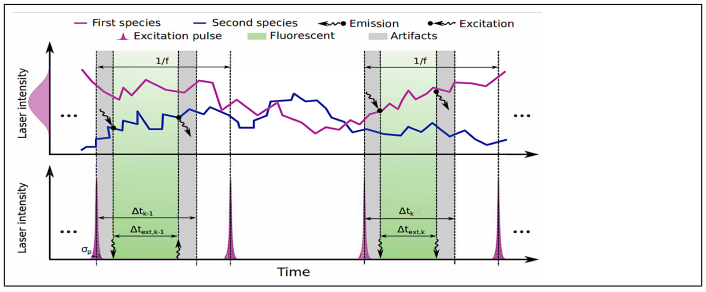
Graphical TOC Entry